Ted Pepins Thesis

TABLE OF CONTENTS

PART II

Last Data = Jan 1968

Preface to Part II

The success of this investigation, like many of the earlier balloon experiments at Minnesota, is in a large part due to the work of the late Ray Maas.

It is the author's sincere hope that he can build upon the foundation of the experimental approach to physics Ray shared with him during the course of his research at Minnesota.

Part II

The Use of Extinction from High Altitude Balloons as a Probe of the Atmospheric Aerosols.

Abstract

This portion of the thesis describes a simple instrument that was developed which measures the intensity of the solar radiation in four spectral regions. Instruments of this type have been used to observe the atmospheric extinction from high altitude balloons at sunrise since mid 1965. The data from these balloon flights is described and the vertical profiles of the atmospheric aerosols determined from these measurements are presented. Evidence is given for a time variation of aerosols at high altitude.

I. Introduction

In the past decade a number of vertical soundings using balloon borne collecting devices and sampling devices have been made to determine the vertical distributio concentration and composition of the atmospheric aerosols. Also, indirect measurements have been made of the aerosols in the stratosphere using optical techniques, e.g. twilight sky intensity measurements, searchlight and laser probing and solar extinction measurements from rockets and satellites From these measurements it has long been realized that the concentration of the aerosols varies in time. Because of the complexity of the collecting and sampling devices and the difficulty of reliably observing the stratospheric aerosols from the surface, it has been difficult to monitor the time variations of this important atmospheric constituent

A small simple optical instrument was developed that measures the extinction of the solar radiation at four wavelengths from a high altitude balloon. From these measurements using the techniques describes in this thesis, the vertical concentration times the effective scattering size of the aerosols can easily be determined. Since the instrument is small and weighs less than 12 pounds it can routinely be carried to high altitudes on 100,000 ft^3 balloons enabling the study of the time variations of the aerosols with relatively small balloons.

II. Description of Equipment and Measurement.

A. Equipment. The balloon borne instrument consists of four telescopes that look in the horizontal direction each with 14 degree x 14 degree fields centered 90 degrees in azimuth from each other. This assembly is rotated beneath the balloon at a constant angular speed of approximately 1 revolution per minute as the balloon floats at constant altitude. During this time the rising sun traverses the vertical fields of the telescopes. The intensity of the solar radiation is measured in four spectral regions as a function of time by the telescopes as they rotate. The intensities are measured to an accuracy of 1%.

The construction details of these telescopes are illustrated in Figure 1. For convenience the telescopes will be referred to as A, B, C and D for the remainder of this thesis. Table 1 summarizes the spectral sensitivities of the telescopes.

Table 1

Telescope	λ [°A]	$\Delta\lambda$ [°A]
A	3670	300
B	4300	350
C	5950	400
D	9100	1400

(λ is wavelength of maximum sensitivity and $\Delta\lambda$ is the full width at one half max sensitivity.)

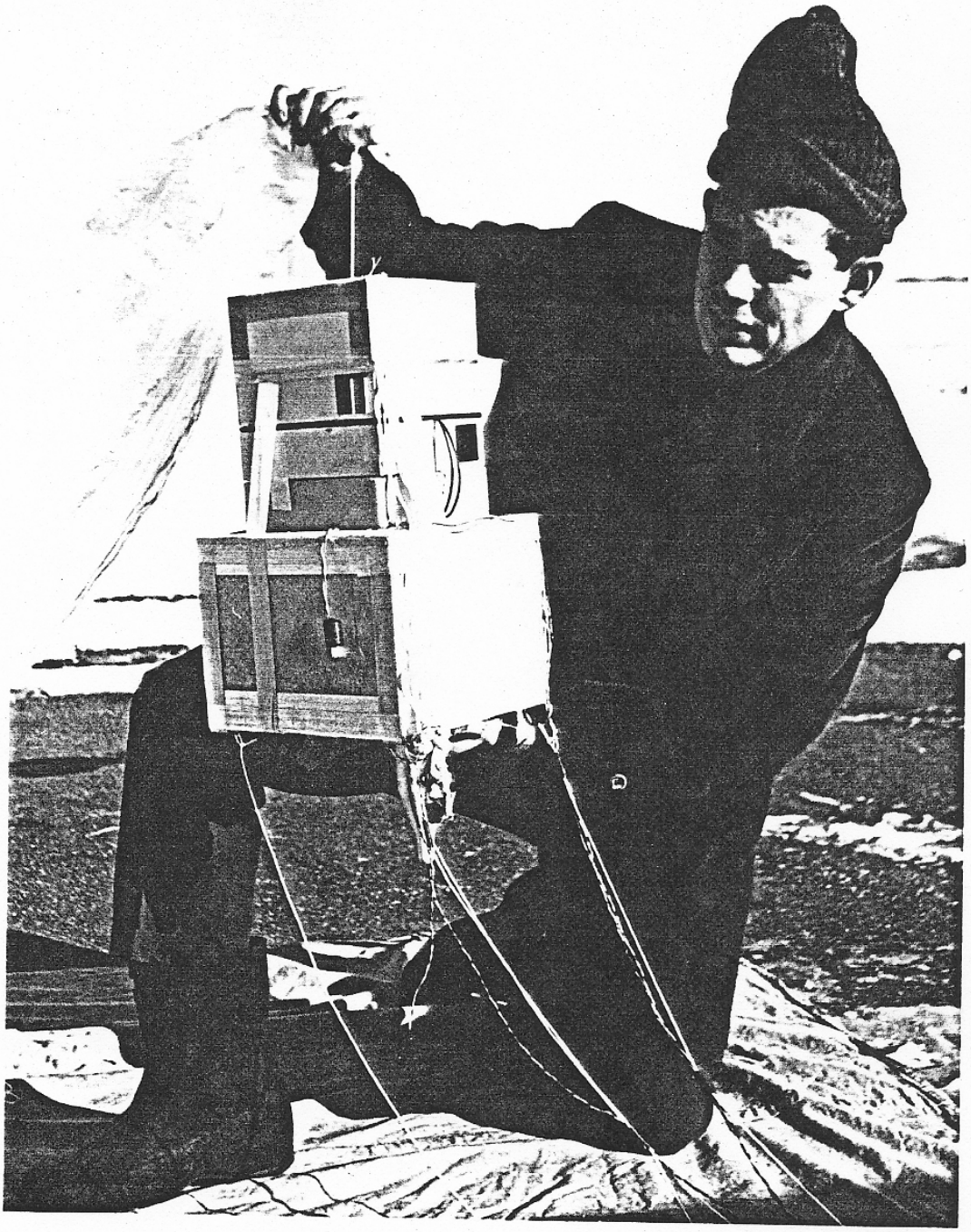

Photograph 1. This photograph shows one of the extinction gondolas attached to the balloon just before launch. The upper portion of the load, near the load line, contains the packaged parachute. The Jones plugs, which were about to be plugged in, turn on the entire experiment which is run from a single battery.

Photograph 2. The short load line and light load simplifies launching. This load can easily be launched by a crew of three and in fact during the course of these experiments on several occasions was launched by only two men.

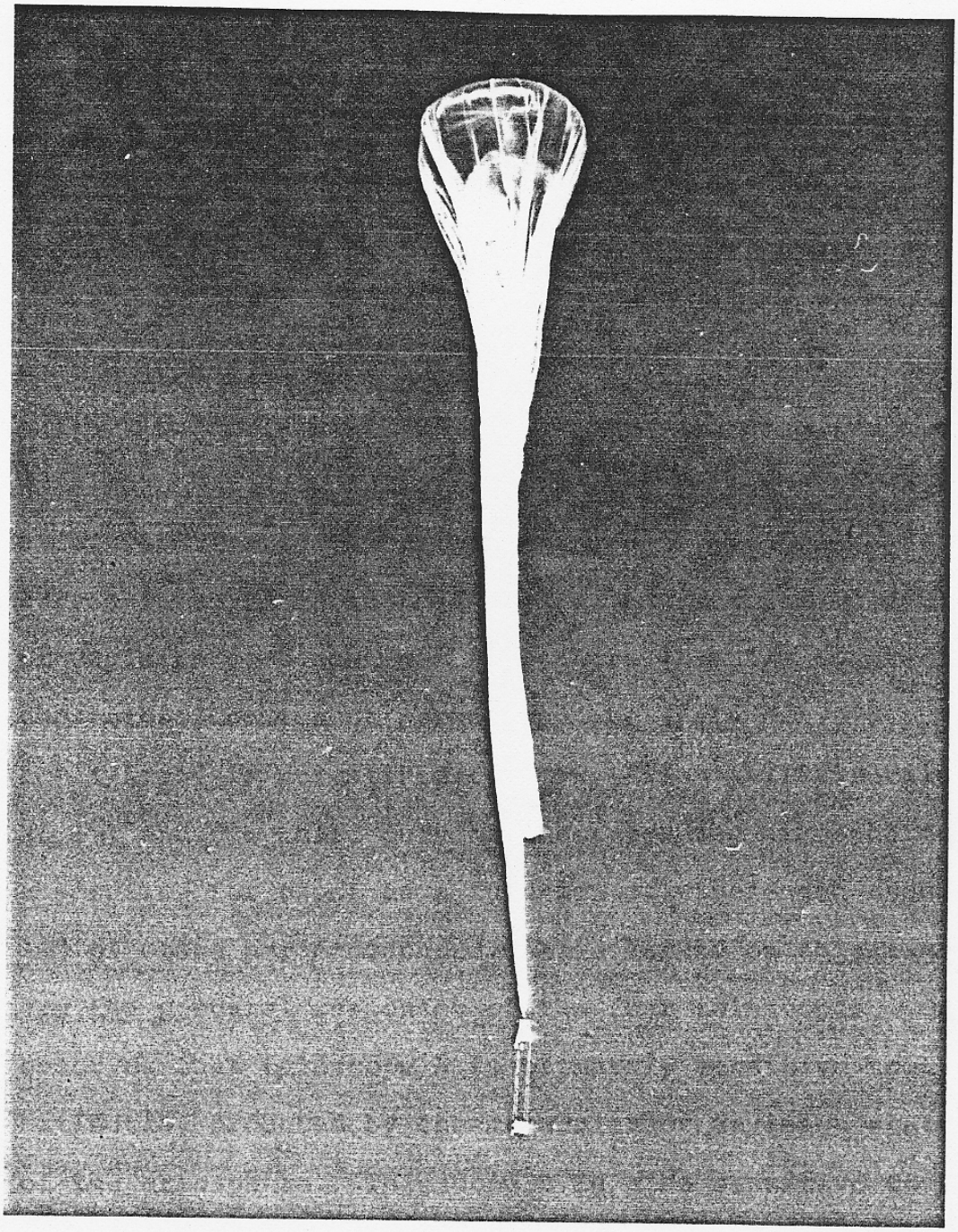

Photograph 3. The balloon and gondola ascending. The load is separated into two packages each weighing less than 6 pounds and tied over 6 feet apart to satisfy the balloon flight regulations for light loads. The lower package only contains the battery.

Telescopes A, B and C employ type 929 vacuum phototubes with S-4 response as detectors. Telescope D uses a type 925 vacuum phototube which has a S-1 response. For each telescope the vignetting curve is measured by scanning over the sun before each flight. This allows one to make a correction for any deviation from a flat response across the field. This correction is less than 4%.

B. Measurement. Figure 2 illustrates the exponential extinction coefficient per atmosphere (k) as a function of wavelength produced by various atmospheric constituents under good average conditions at sea level. There are three curves illustrated in this figure, one for the molecular or Rayleigh component per atmosphere ($k \propto 1/\lambda^4$), one for the aerosol component per atmosphere (this curve assumes $k \propto 1/\lambda$ and is normalized to C. W. Allen's (1963) value at 1μ) and the third curve illustrates the atmospheric absorption for ozone as a function of wavelength assuming 3mm of ozone per atmosphere. Also marked on this figure are the spectral responses of the four telescopes. One observes that telescope A is primarily sensitive to the extinction produced by the molecular or Rayleigh scattering of the atmosphere. Telescope B is also sensitive to the Rayleigh component and to some extent the extinction produced by the atmospheric aerosols. Telescope C is centered in the middle of the Chappuis bands of ozone. Along with being sensitive to extinction produced by the molecular and aerosol components of the atmosphere it is

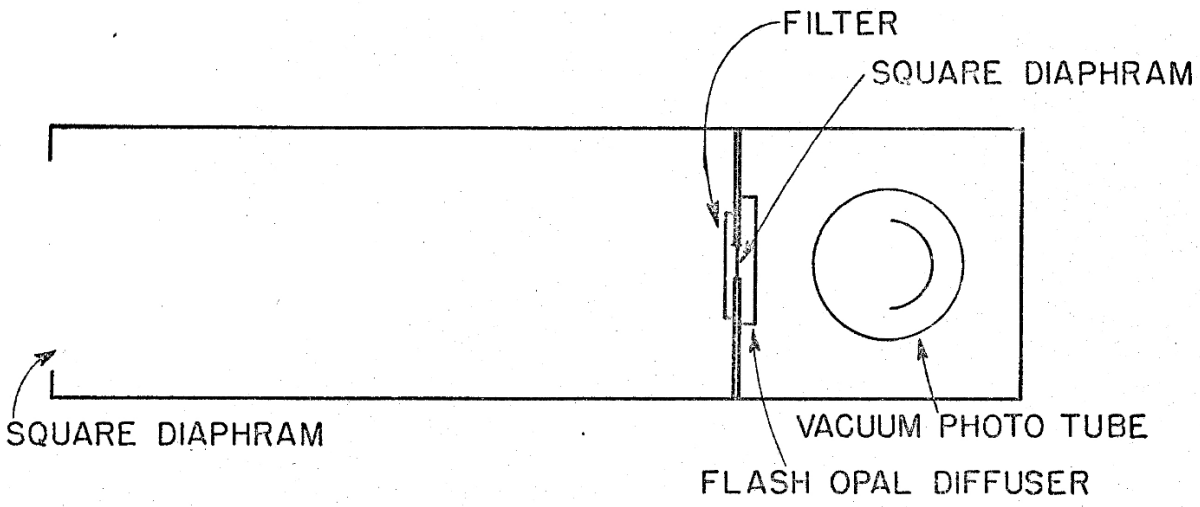

Construction details of telescope used in extinction measurements.

Figure 1

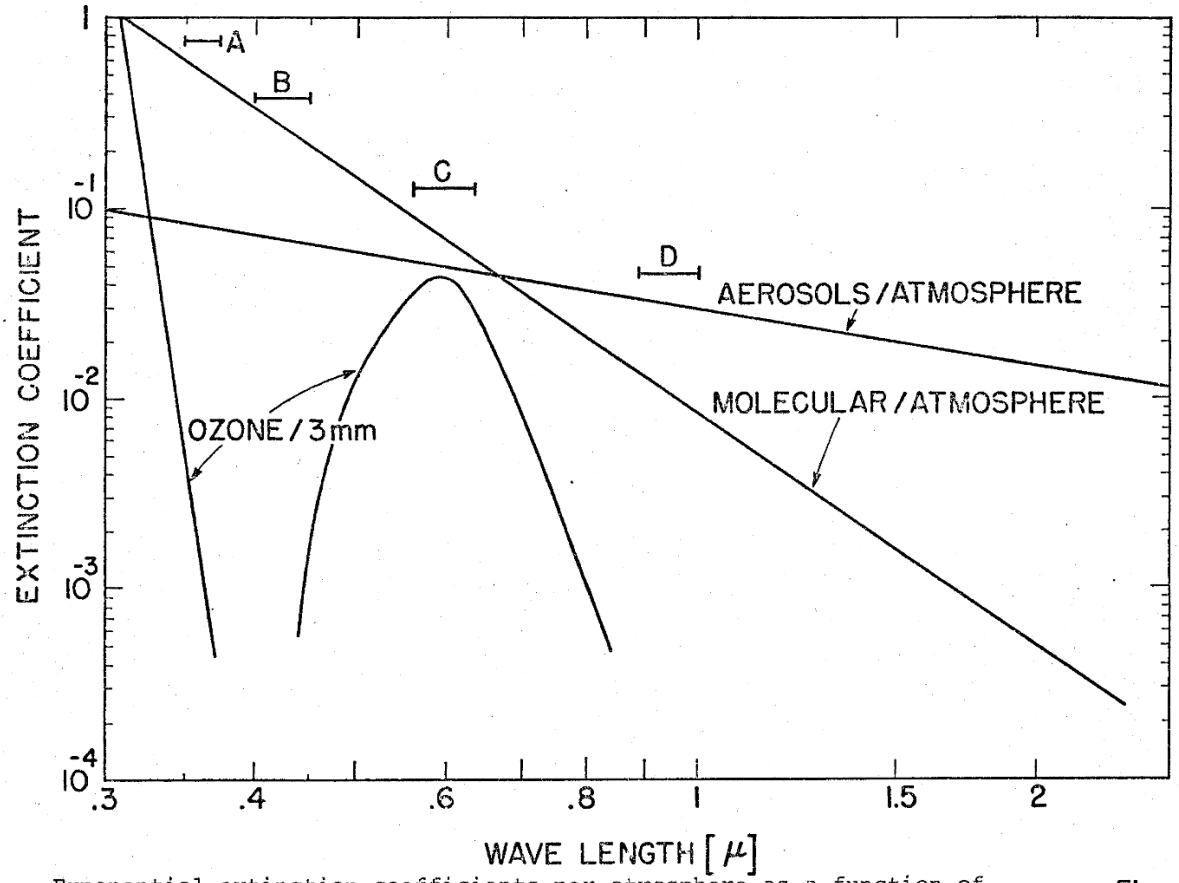

Exponential extinction coefficients per atmosphere as a function of wavelength. Spectral sensitivities of the telescopes are noted.

Figure 2

sensitive to absorption caused by the Chappuis bands. Telescope D is primarily sensitive to the extinction caused in the atmosphere due to the presence of the atmospheric aerosol component.

Figure 3 demonstrates the intensity that one would expect to observe as a function of atmospheric path for each of the four telescopes assuming a pure molecular atmosphere.

From the flight of April 12, 1967, Figure 4 has been constructed by plotting the observed intensity from each of the telescopes as a function of the calculated air mass (air mass calculations will be described in the next section). One observes the similarity of the data from telescopes A and B to that expected for a Rayleigh atmosphere whereas the data of telescopes C and D appear different. The difference in the data of telescope C from that expected for a Rayleigh atmosphere is a reflection of the extinction produced by the ozone component of the atmosphere. The inflection in the data from telescope D between 5 and 8 atmospheres is produced by an increased concentration of atmospheric aerosols above the tropopause as will be discussed in later sections.

III. Calculation of Air Mass.

In order to plot the telescope data as a function of air mass, one must calculate the atmospheric air mass traversed by the solar ray before it enters the telescope.

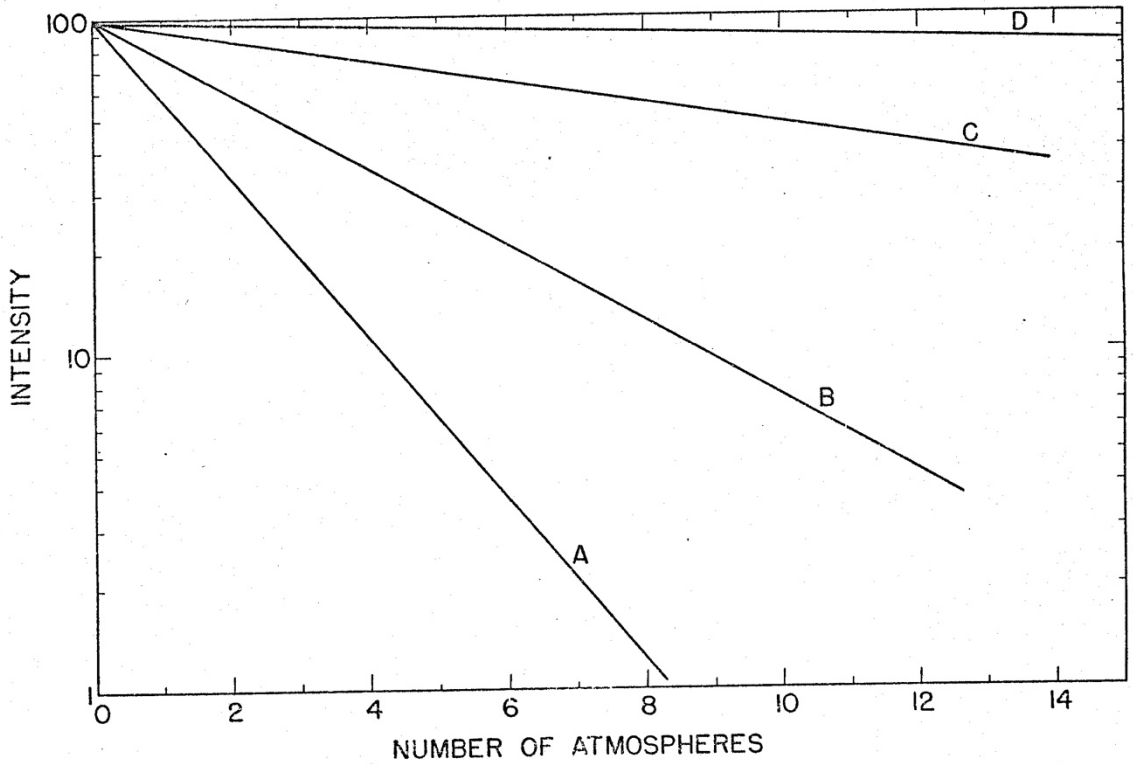

Theoretical intensity as a function of atmospheric path for the four telescopes in a pure Rayleigh atmosphere.

Figure 3

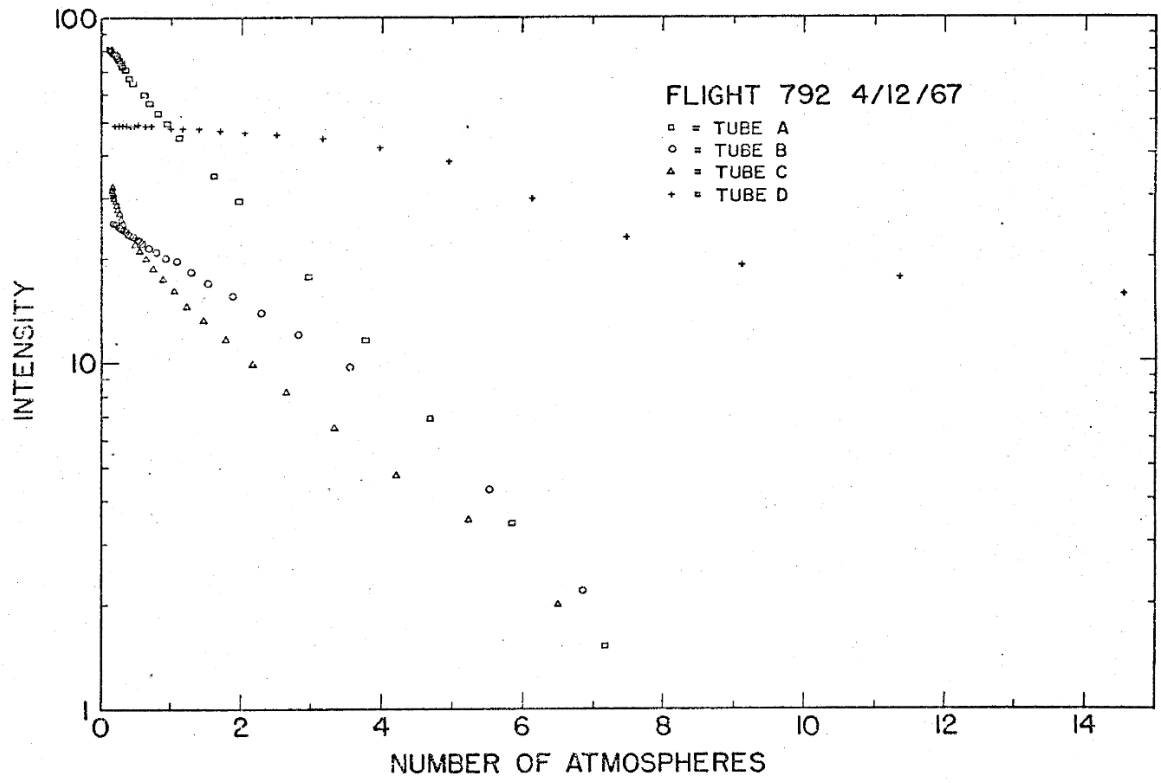

Intensity as a function of atmospheric path for Flight 792.

Figure 4

A knowledge of the position of the balloon as a function of time, which is determined from the pressure measured using an Olland cycle on the balloon and from tracking the balloon using a G.M.D., enables one to determine by the use of the Air Almanac the true elevation angle (α) of the sun as a function of time. The air mass can then be calculated knowing the elevation angle of the sun and the geometric altitude of the balloon (h_B). The geometry of the calculation is illustrated in Figure 5. α is negative for elevation angles below the horizontal direction.

A. Positive Elevation Angles. For positive elevation angles, the air mass traversed by a solar ray before entering the telescope at altitude of h_B when the sun is at elevation angle α is given by:

$$A(\alpha,h_B) = A(\alpha,0) \frac{P(h_B)}{P(0)} \text{ , for } \alpha \geq 0 \qquad (1)$$

where $P(h)$ is the pressure at altitude h and $A(\alpha,0)$ is the number of air masses from the surface at elevation angle α without the correction for refraction. Since the refraction at positive elevation angles is proportional to the density at the balloon's altitude, the correction for refraction does not significantly influence relation(1) and need not be considered for positive elevation angles.

The surface air mass $A(\alpha,0)$ has been measured and calculated for various model atmospheres by a number of authors. (A good review of the determination of $A(\alpha,0)$ has been presented by Rozenberg (1966)). For the present study the author has used the air mass tabulated by Allen (1963).

B. Negative Elevation Angles. For negative elevation angles one can calculate the air mass traversed by the solar beam before reaching the telescope by observing that at the tangent height of the ray, h_T, the air mass to the tangent point is given by:

$$A(0,h_T) = A(0,0) \frac{P(h_T)}{P(0)} \qquad (2)$$

But, the total air mass at elevation angle $-\alpha$ is just twice the air mass to the tangent point minus the air mass at $+\alpha$. OR

$$A(-\alpha,h_B) = 2A(0,0) \frac{P(h_T)}{P(0)} - A(\alpha,0) \frac{P(h_B)}{P(0)} . \qquad (3)$$

In relations (2) and (3), h_T is the height of the tangent ray which is affected by refraction. Its height can be calculated by an iterative procedure.

C. Calculation of Tangent Height. From Figure 5 it may be seen that the tangent height of a ray with no

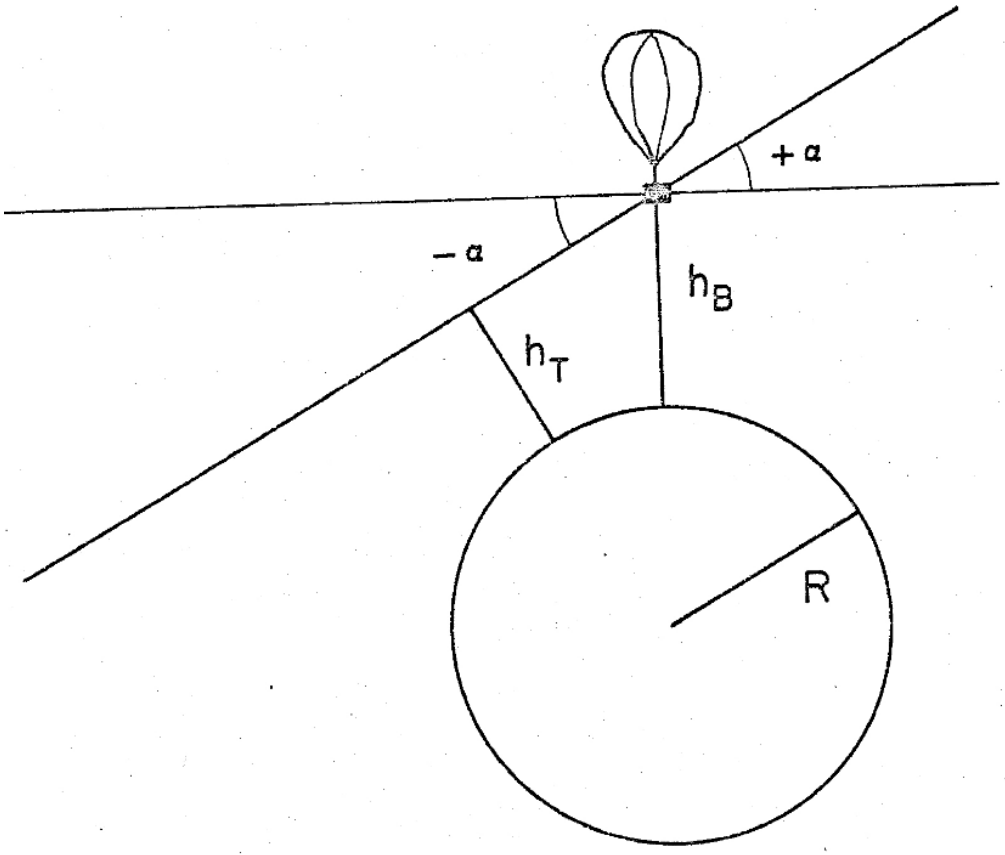

Geometry of the air mass calculation.

Figure 5

refraction is given by

$$h_T = h_B \cos \alpha - R (1-\cos \alpha) \qquad (4)$$

where R is the radius of the earth. From the tangent height for a straight ray (no refraction) the first estimat of the pressure of the true tangent altitude is determined, and thus the first estimate of the air mass (A') to the tangent point traversed by the ray, using equation (2). The refraction of the tangent ray to the tangent point is then calculated as

$$\beta = \beta_o A' \frac{1}{.965 + .0035 T(h_T)} \qquad (5)$$

where $T(h_T)$ is the temperature at altitude h_T in degrees centigrade. In equation (5), which is due to C. W. Allen (1963), β_o is the refraction per air mass and for the wavelengths used in these experiments has the numerical value 1 min of arc per air mass.

Since β is a small angle and most of the refraction occurs near the tangent altitude one may obtain a second estimate of h_T from equation (4) by substituting for α the apparent elevation angle $-\alpha + \beta$.

Having thus calculated the tangent height, corrected for refraction to first order, relation (2) can again be

used to calculate the air mass corrected for refraction to first order and then the calculation of the tangent height can be repeated and the iterative procedure can be continued.

A good check on the calculation of the tangent height is offered by the data itself. It is observed that in flights made at times of good weather that the signal of telescope D is first observed at the time when one would just predict the sun had come over the limb of the earth. If one calculates the tangent height at the time the first signal is observed using the above method he finds it is only a fraction of a km indicating the correction for refraction has been applied correctly to first order.

IV. Determination of $N\sigma(h)$ from Extinction Data.

The number density times the effective scattering size of the atmospheric aerosols as a function of altitude, $N\sigma(h)$, can be determined from the extinction data from telescope D by considering a model atmosphere consisting of a number of layers and working out the extinction produced in each of the layers as the solar rays traverse them.

A. Calculation of Path Lengths. The atmosphere below the balloon is conveniently divided into a number of layers by the tangent heights of the observed rays when the sun is below the horizon. It is convenient to index the layers from the balloon down from 1 to k

and assign the index 0 to the layer above the balloon of thickness S which is assumed to contain the aerosols above the balloon. The tangent height, h_k, can be calculated by the method outlined in the previous section and the geometry is illustrated in Figure 6. The path lengths P_{jk} of the jth ray in the kth layer can be calculated from simple geometry and it is found:

$$P_{oo} = [S \{S + 2 (h_o + R)\}]^{1/2} \tag{6}$$

where R is the radius of the earth,

$$P_{jo} = [(h_o + S - h_j) (h_o + S + h_j + 2R)]^{1/2} - [(h_o - h_j) (h_o + h_j + 2R)]^{1/2} \tag{7}$$

and for $k > 0$

$$P_{jk}=2[(h_{k-1} - h_j)(h_{k-1} + h_j + 2R)]^{1/2} - \sum_{\substack{i=k+1 \\ i\neq j}}^{j} P_{ji} \tag{8}$$

B. $N\sigma(h)$. Invoking the Lambert-Beer law one has the intensity I of the light ray after traversing a path length P when the incident intensity is I' as:

$$I = I' e^{-N \sigma P} \tag{9}$$

where N is the number of scattering centers per unit

volume and σ is the effective cross-section of the average scattering center.

By plotting the observed intensity from telescope D corrected for the Rayleigh component as a function of air mass one can extrapolate to find the intensity at the top of the atmosphere, $I_\odot$, and with the observed intensity corrected for the Rayleigh component in the horizontal direction, I_0, one can invert relation (9) to find

$$(N\sigma)_o = \frac{\log_e \frac{I_\odot}{I_0}}{P_{oo}}$$

by using relation (6) to calculate P_{oo}.

Having determined $(N\sigma)_o$, one can trace the first ray below the horizontal through the atmosphere, again using relation (9) along with (7) and (8) to find

$$(N\sigma)_1 = \frac{\log_e \frac{I_\odot}{I_1} - (N\sigma)_o P_{10}}{P_{11}} .$$

One can continue to solve for the $(N\sigma)_k$'s using the measured intensities corrected for the Rayleigh component, I_k, for successive lower layers and in general one finds

$$(N\sigma)_k = \frac{\log_e \frac{I_\odot}{I_k} - \sum_{i=0}^{k-1} (N\sigma)_i \; P_{ki}}{P_{kk}}$$

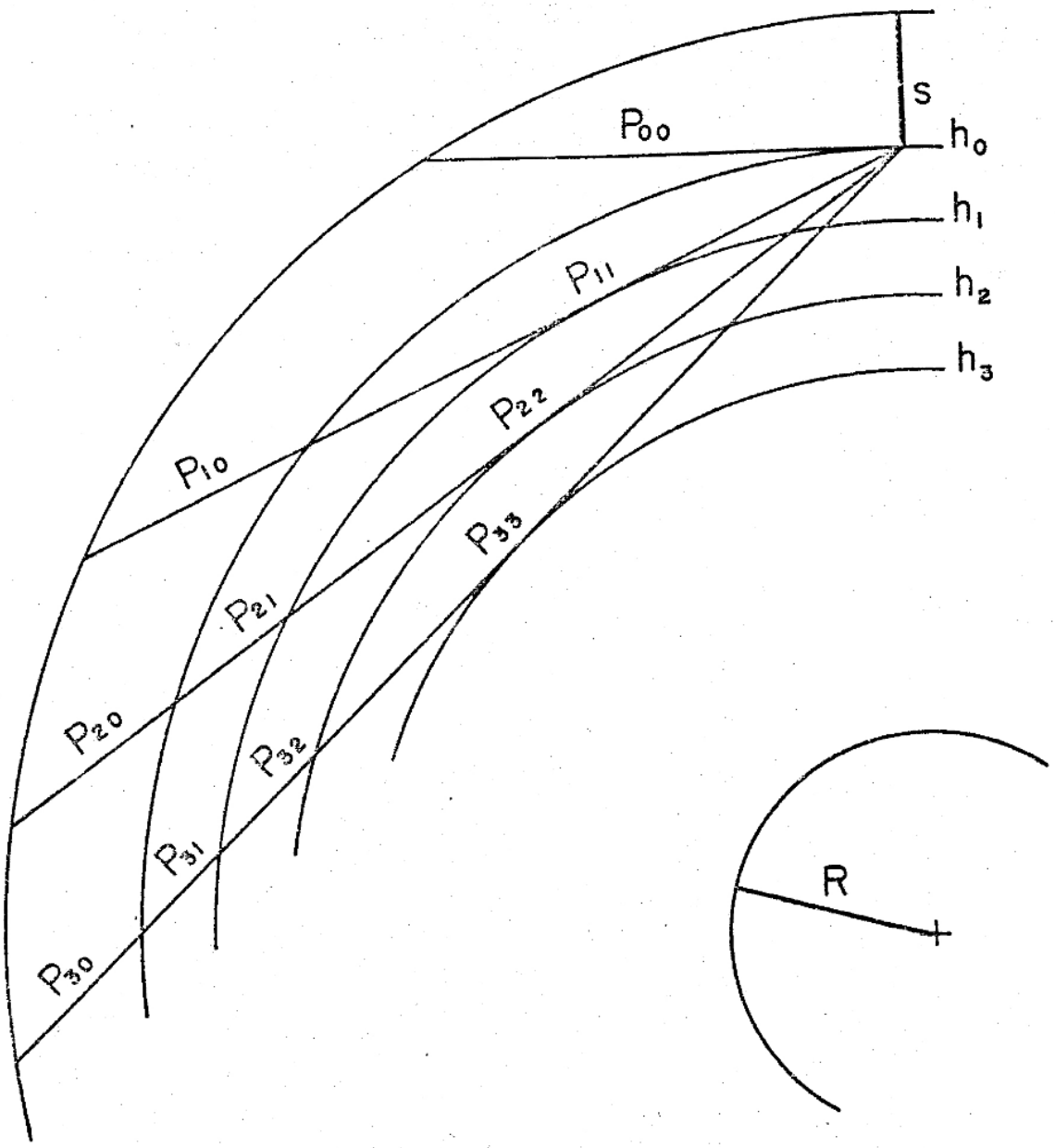

Geometry in a layered atmosphere used for determining $N\sigma(h)$.

Figure 6

In order to carry out the above calculation one can assume a value for S. In the present work S was first assumed to be the atmospheric scale height and then after the calculation was completed the assumption was made that σ was independent of altitude and the scale height of the aerosols was determined. This scale height was then used for S and the calculation repeated. Since a balloon at an altitude of 32 km is above almost all of the aerosols the choice of S does not critically influence the results.

As a test of the consistency of this method in one of the balloon flights of this series telescope C was replaced with a telescope D so that there were two identical telescopes looking in the infrared wavelength on the same flight. The data from these telescopes were analyzed independently and are plotted in Figure 7. Both are seen to give the same result.

V. Data from Extinction Flights.

From the summer of 1965 to early 1968 a number of extinction flights were made from Minneapolis and one flight (774) was made from the Panama Canal Zone. These flights are summarized in Table II.

Table II

Flight Number	Date	Flight Number	Date
751	7/13/65	782	1/19/67
754	7/28/65	783	2/1/67
761	11/20/65	786	2/24/67
765	6/7		
767	7/29/66	788	3/10/67
768	8/3/66	791	4/1/67
770	8/24/66	792	4/12/67
771	9/6/66	793	4/28/67
772	9/15/66	794	5/10/67
774*	9/14/66	798	6/21/67
779	12/23/66	801	7/12/67
780	12/30/66	813	1/18/68

* Panama

Panama = Sept 12/14

The data from these flights have been analyzed using the method outlined in the above sections and $N\sigma(h)$ has been determined at the time of each of the measurements. Figures 8 through 29 illustrate the $N\sigma(h)$'s determined in these measurements. In these figures the $(N\sigma)_k$'s have been plotted vs. the tangent height h_k for the kth layer. The curved grid lines on the background of these figures are proportional to lines of constant mixing ratios for the atmospheric aerosols if the effective scattering cross-section is independent of altitude. The numerical values on the lines, thus interpreted, are proportional to the mixing ratio.

In this series of flights the highest concentration of aerosols above the tropopause at Minneapolis was observed in Flight 780 on December 30, 1966. The observed N in this layer was 6×10^{-8} cm^{-1}. If one assumes the average radius of the aerosols responsible for the extinction was .5μ, one calculates the concentration of aerosols in this layer to be $4/cm^3$.

An even greater extinction by the atmospheric aerosols ($N\sigma > 6 \times 10^{-8}$ cm^{-1}) was observed in Flight 774 made in Panama. This flight was made at the same time that J. M. Rosen (1968) made direct soundings of the atmospheric aerosols. He too found a high concentration of aerosols at this time in the stratosphere above Panama.

VI. Discussion of Results.

A. Variability of the Stratospheric Aerosols.

Study of Figures 7-29 reveals the variability of the aerosol concentration in the stratosphere and in a layer just above the tropopause. This layer is often seen to contain an increased aerosol concentration. These variations are in fact systematic in time as is evidenced by Figure 30. In this figure the extinction coefficient k_{IR}, determined from the data of the D telescope from each flight when the solar ray traversed one atmospheric air mass, is plotted above the date of each flight. As has been pointed out in earlier sections, k_{IR}, the extinction coefficient, is proportional to the

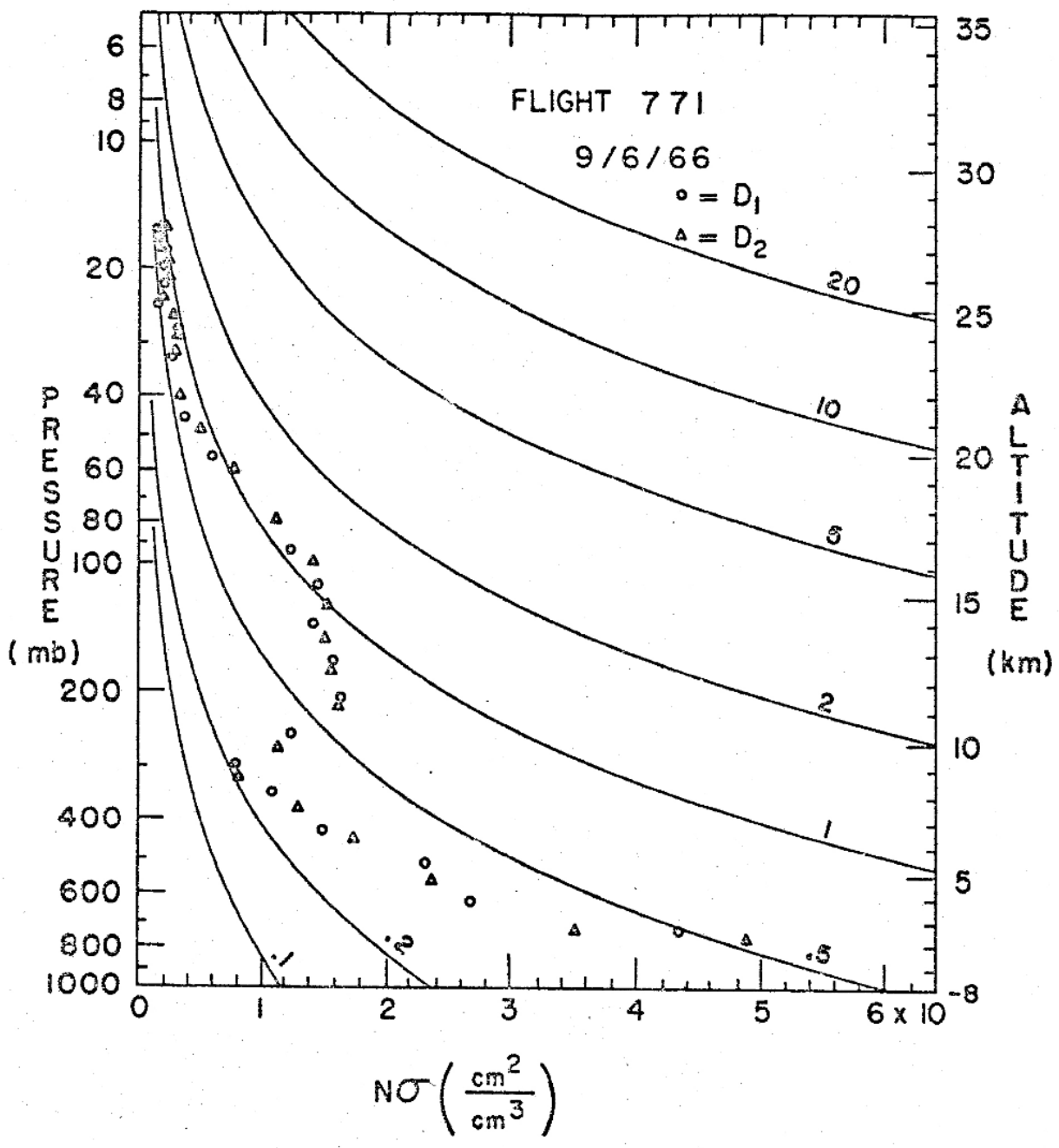

Nσ(h) for the flight of September 6, 1966. Data is plotted which was determined independently from two different telescopes.

Figure 7

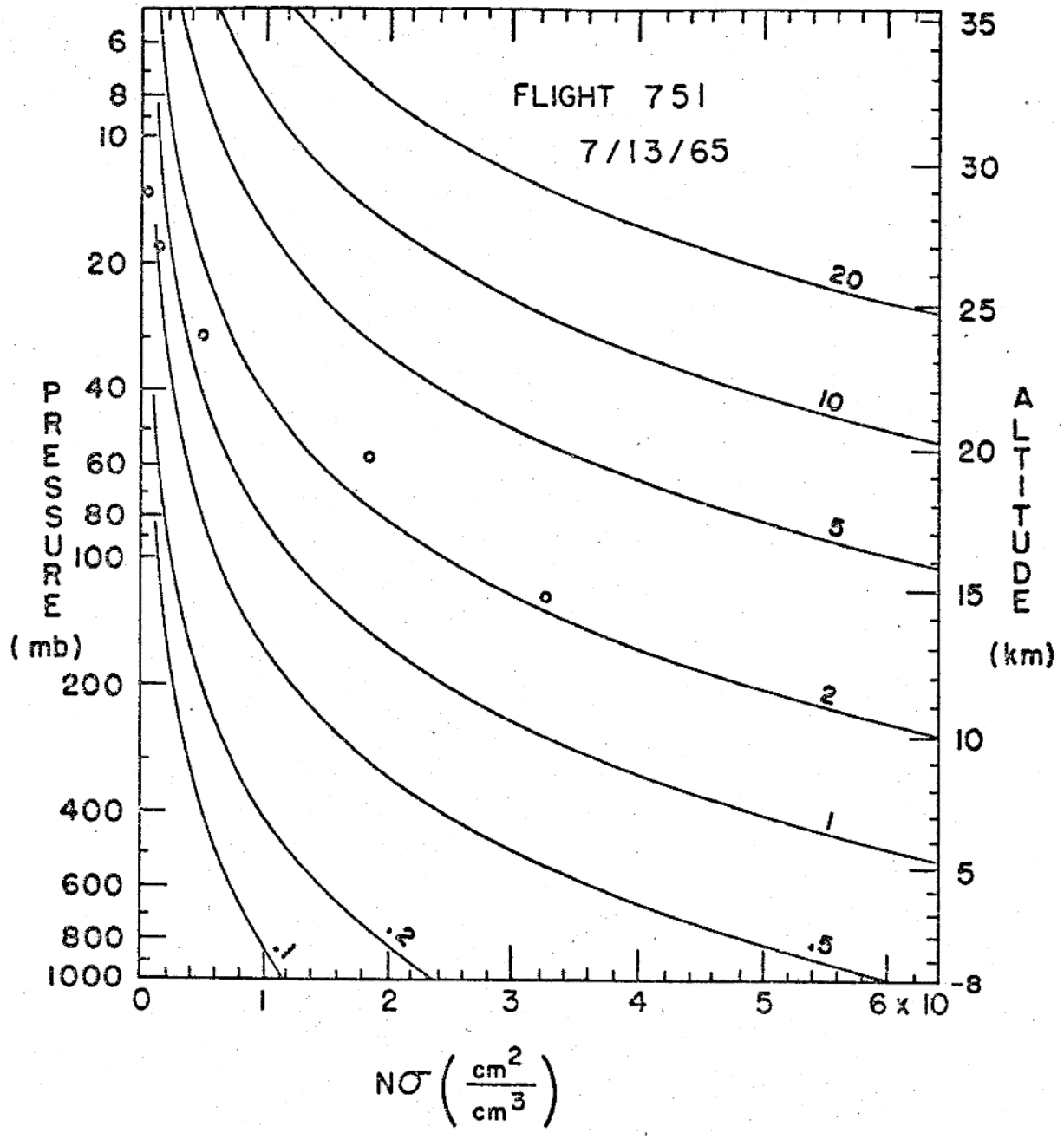
FLIGHT 751
7/13/65
PRESSURE (mb)
ALTITUDE (km)
6
8
10
20
40
60
80
100
200
400
600
800
1000
35
30
25
20
15
10
5
-8
20
10
5
2
1
.5
.2
.1
0
1
2
3
4
5
6 x 10
NO (cm²/cm³)

Figure 8

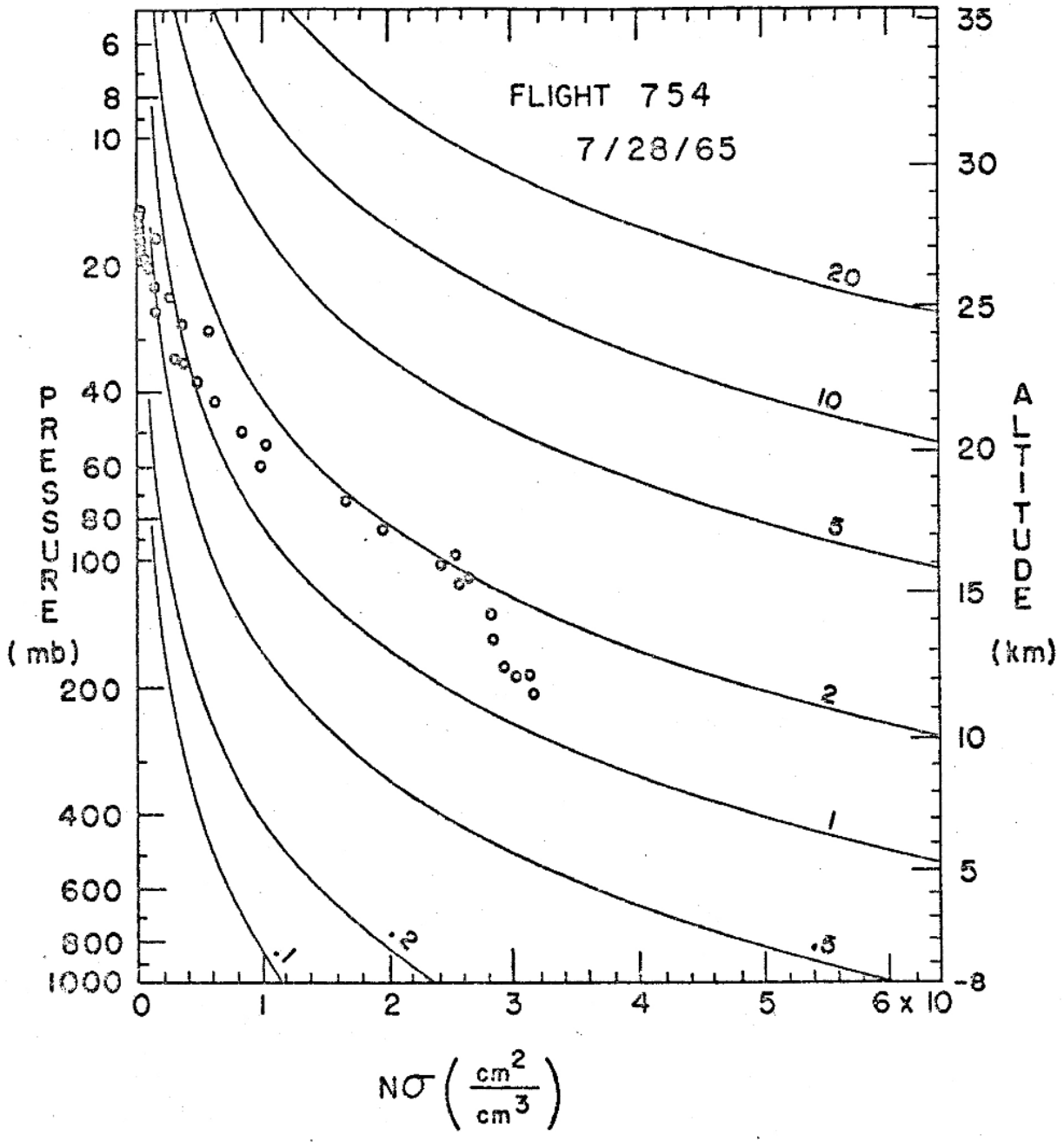
FLIGHT 754
7/28/65
PRESSURE (mb)
ALTITUDE (km)
6
8
10
20
40
60
80
100
200
400
600
800
1000
35
30
25
20
15
10
5
-8
20
10
5
2
1
.5
.2
.1
0
1
2
3
4
5
6 x 10
$N\sigma\left(\frac{cm^2}{cm^3}\right)$

Figure 9

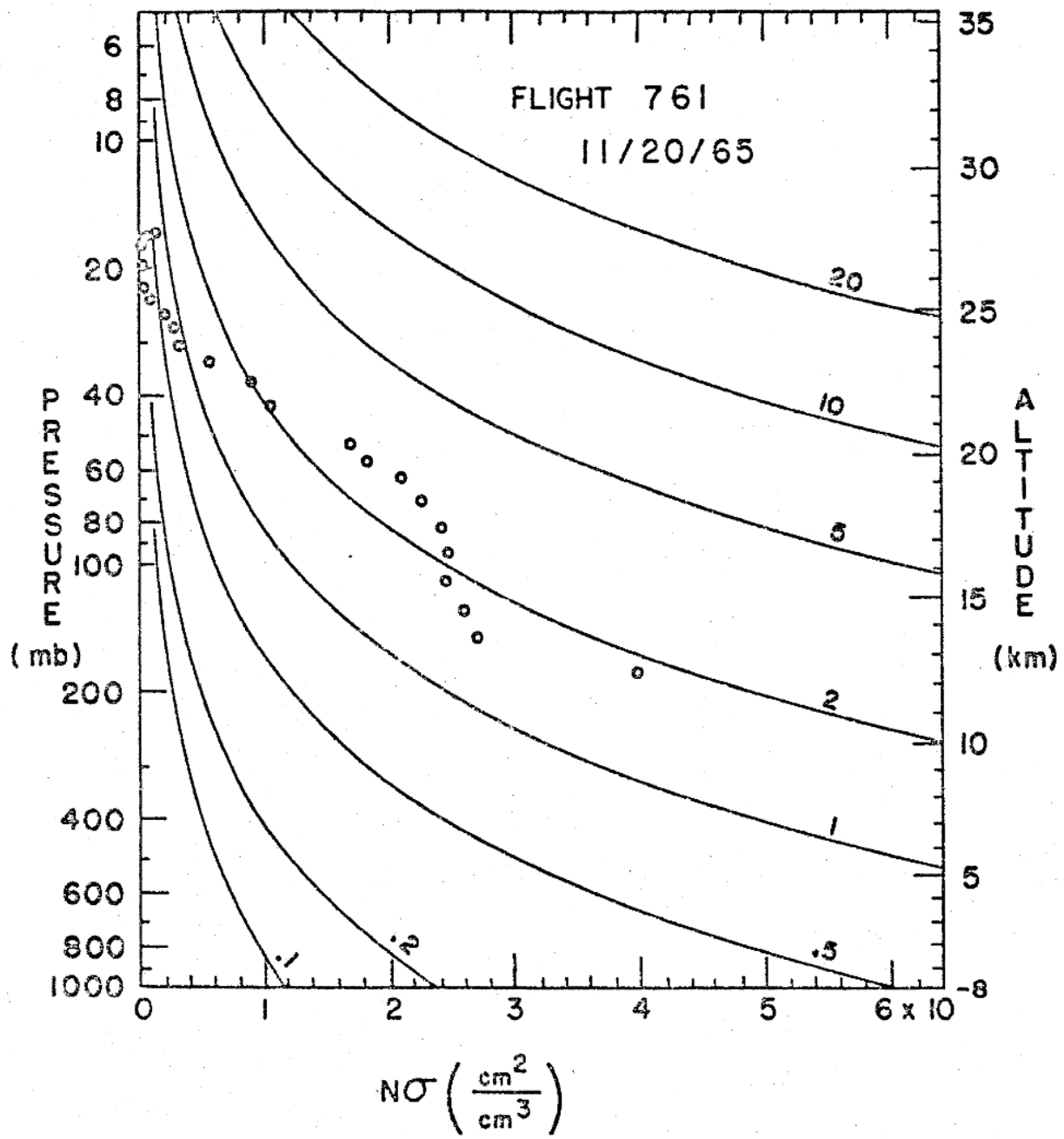
FLIGHT 761
11/20/65
PRESSURE (mb)
ALTITUDE (km)
6
8
10
20
40
60
80
100
200
400
600
800
1000
35
30
25
20
15
10
5
-8
20
10
5
2
1
.5
.2
.1
0
1
2
3
4
5
6 x 10
Nσ (cm²/cm³)

Figure 10

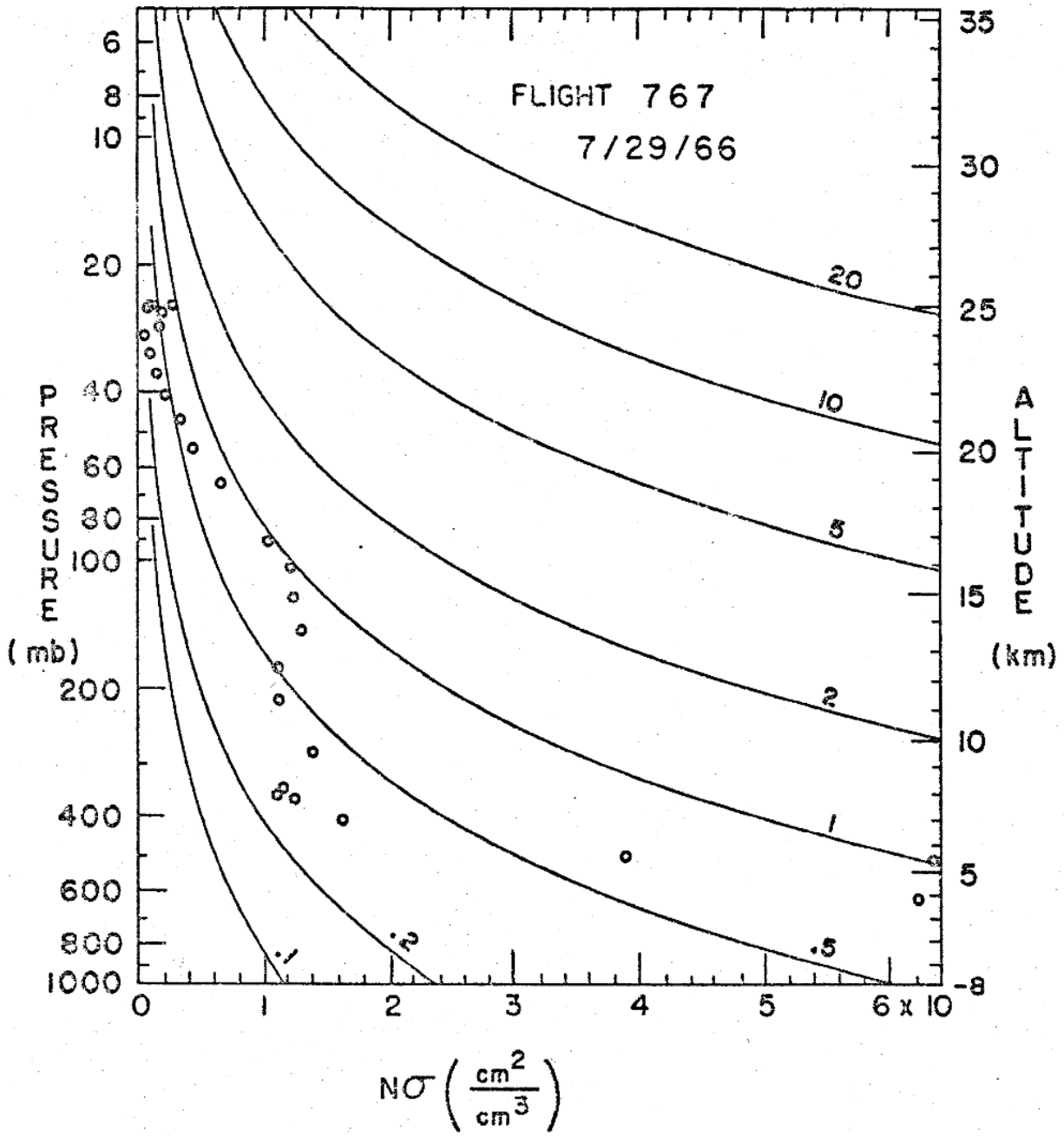
FLIGHT 767
7/29/66
PRESSURE (mb)
ALTITUDE (km)
6
8
10
20
40
60
80
100
200
400
600
800
1000
35
30
25
20
15
10
5
-8
20
10
5
2
1
.5
.2
.1
0
1
2
3
4
5
6 x 10
Nσ (cm²/cm³)

Figure 11

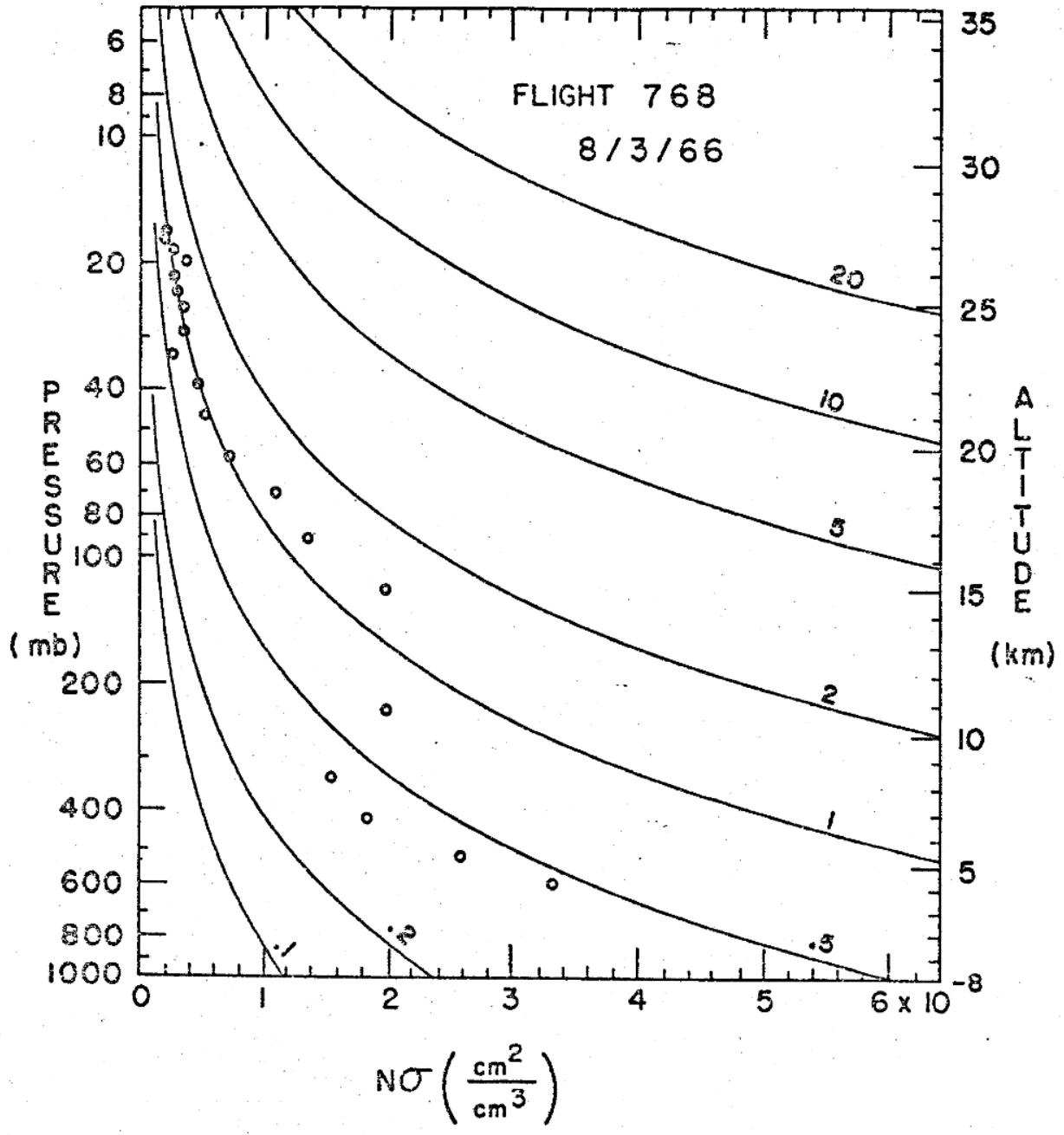
FLIGHT 768
8/3/66
PRESSURE (mb)
ALTITUDE (km)
6
8
10
20
40
60
80
100
200
400
600
800
1000
35
30
25
20
15
10
5
-8
20
10
5
2
1
.5
.2
.1
0
1
2
3
4
5
6 x 10
$N\sigma\left(\frac{cm^2}{cm^3}\right)$

Figure 12

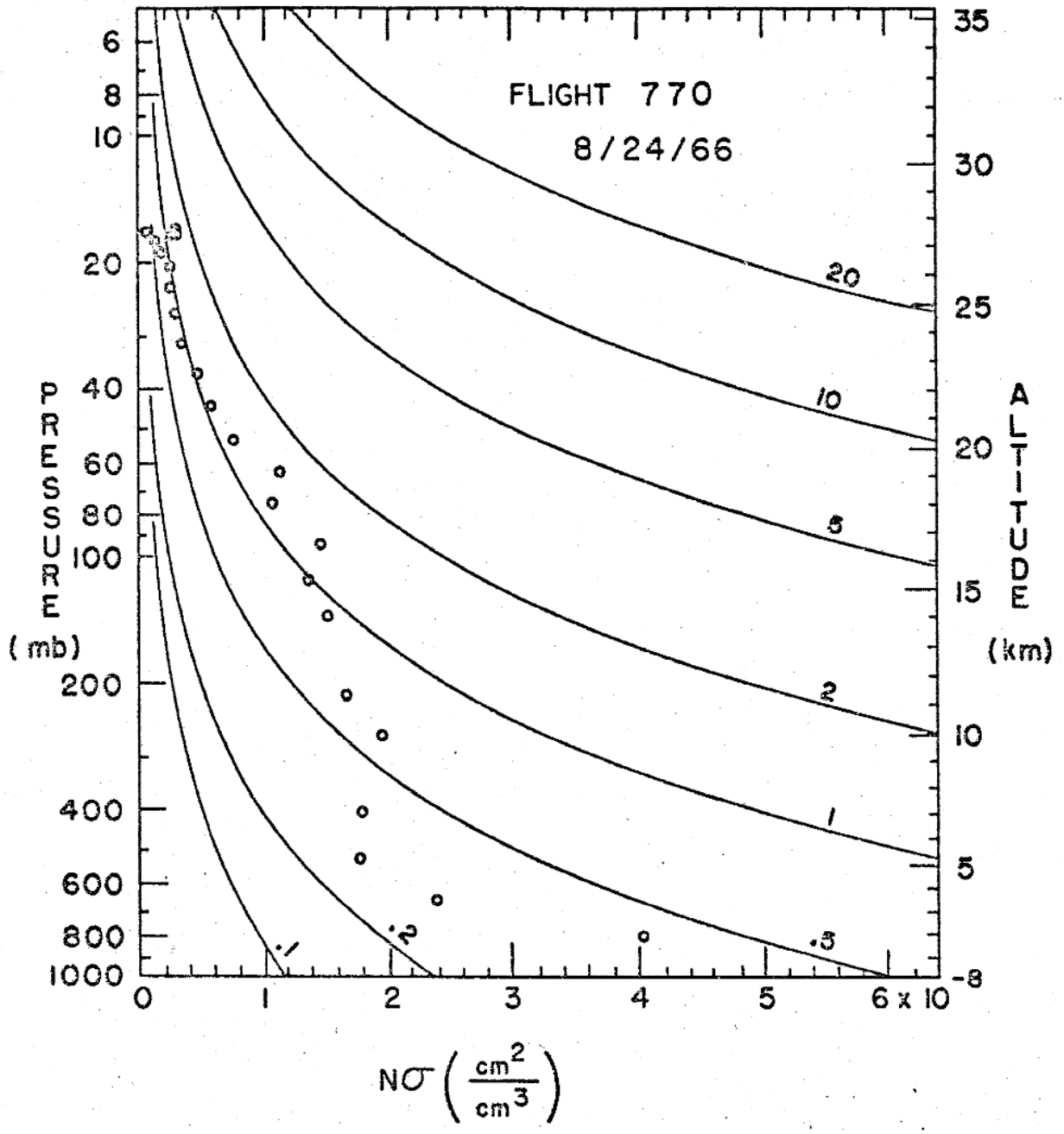
FLIGHT 770
8/24/66
PRESSURE (mb)
ALTITUDE (km)
6
8
10
20
40
60
80
100
200
400
600
800
1000
35
30
25
20
15
10
5
-8
20
10
5
2
1
.3
.2
.1
0
1
2
3
4
5
6 x 10
NσT (cm²/cm³)

Figure 13

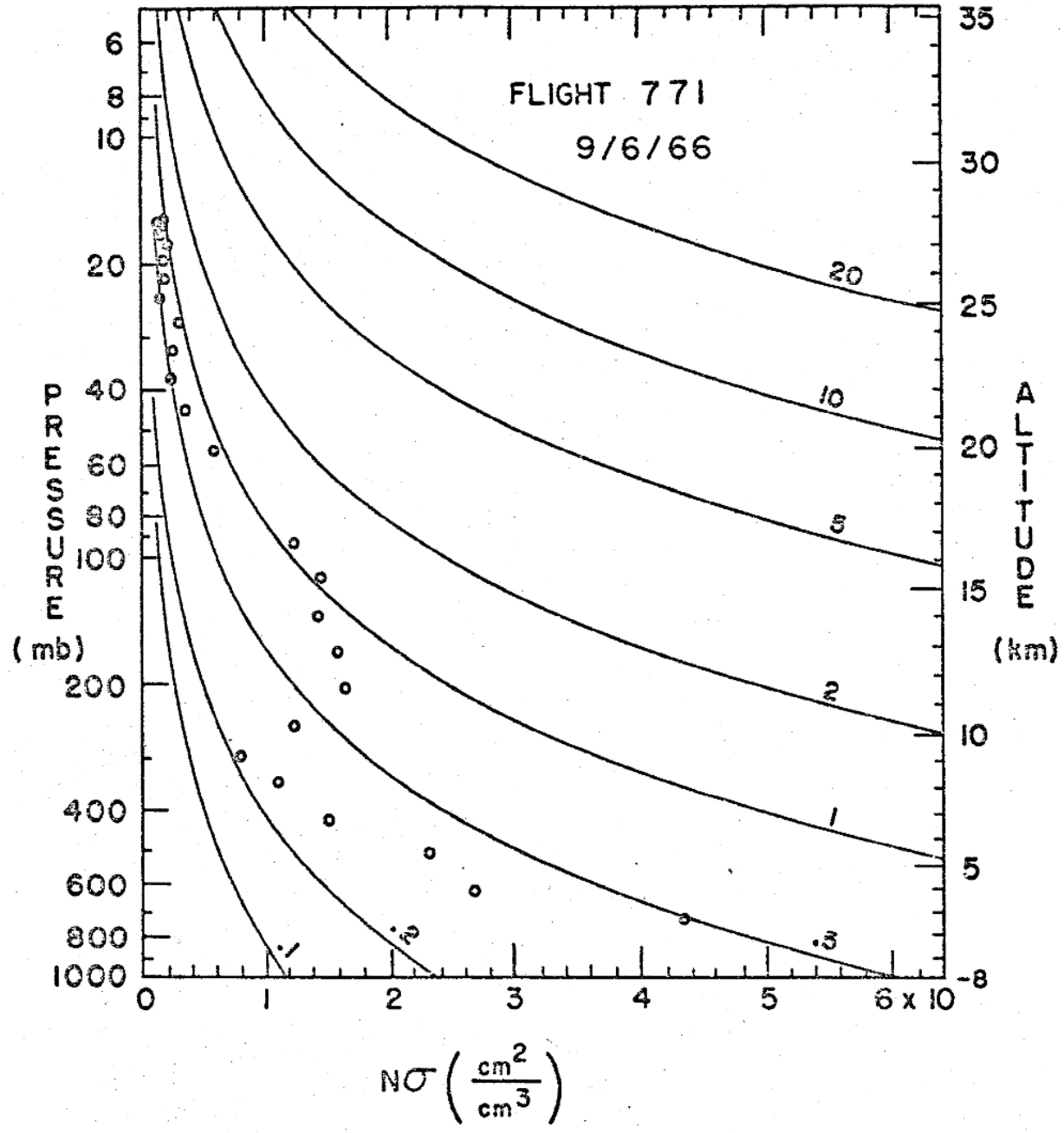
FLIGHT 771
9/6/66
PRESSURE (mb)
ALTITUDE (km)
6
8
10
20
40
60
80
100
200
400
600
800
1000
35
30
25
20
15
10
5
-8
20
10
5
2
1
.3
.2
.1
0
1
2
3
4
5
6 x 10
$N\sigma\left(\frac{cm^2}{cm^3}\right)$

Figure 14

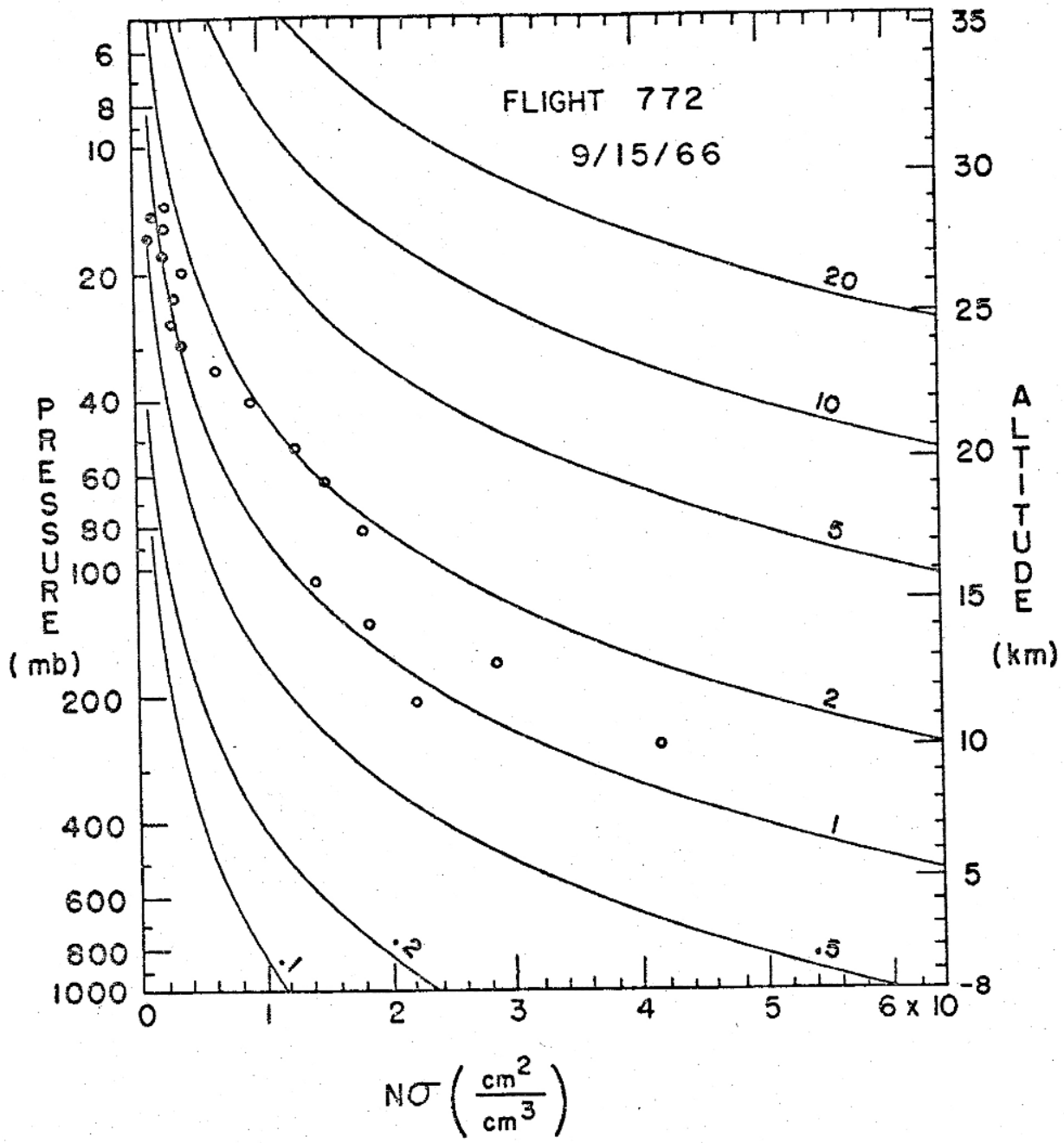
FLIGHT 772
9/15/66
PRESSURE (mb)
ALTITUDE (km)
6
8
10
20
40
60
80
100
200
400
600
800
1000
35
30
25
20
15
10
5
-8
20
10
5
2
1
.5
.2
.1
0
1
2
3
4
5
6 x 10
NσT (cm²/cm³)

Figure 15

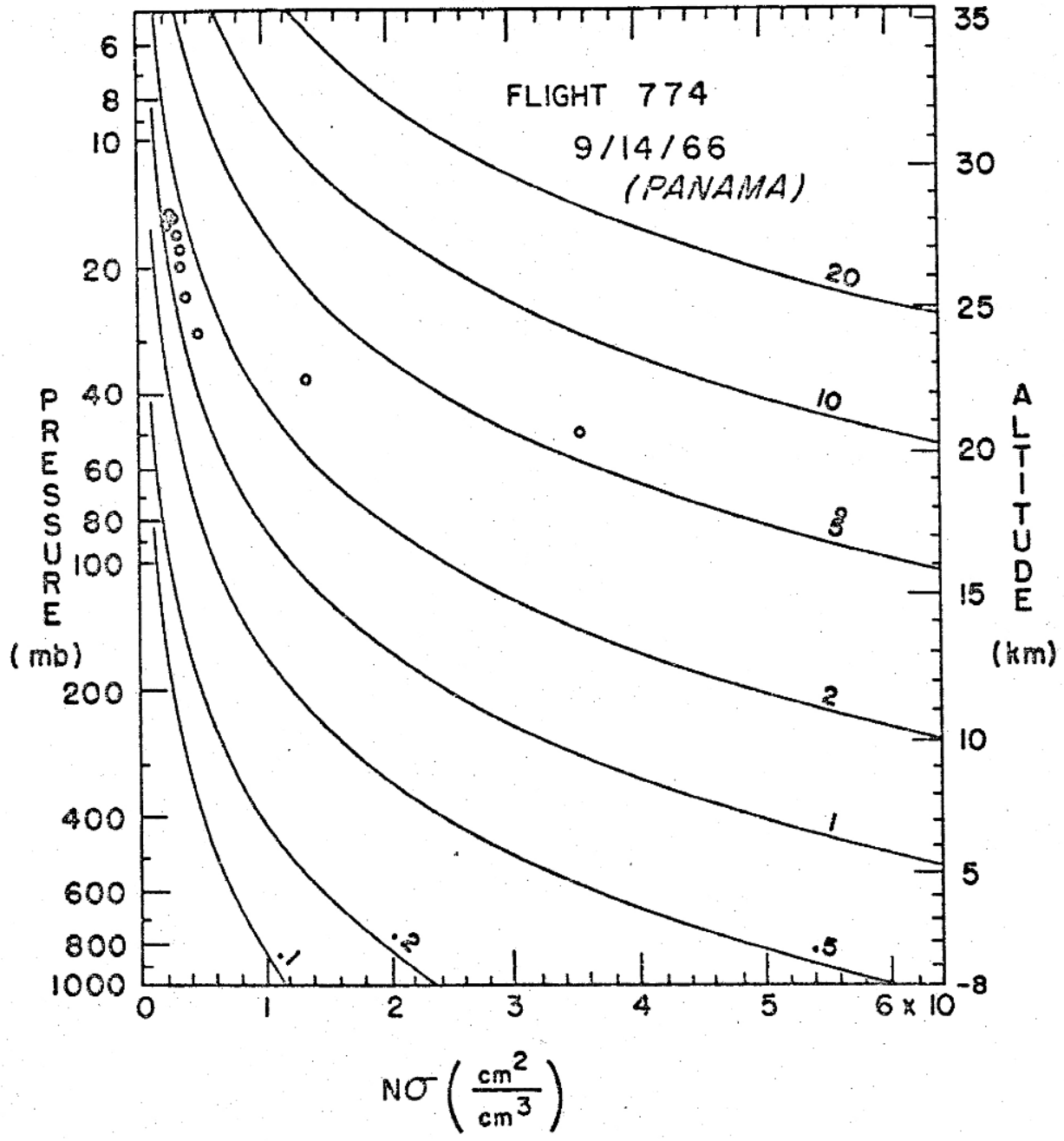
FLIGHT 774
9/14/66
(PANAMA)
PRESSURE (mb)
ALTITUDE (km)
6
8
10
20
40
60
80
100
200
400
600
800
1000
35
30
25
20
15
10
5
-8
20
10
3
2
1
.5
.2
.1
0
1
2
3
4
5
6 x 10
NσT (cm²/cm³)

Figure 16

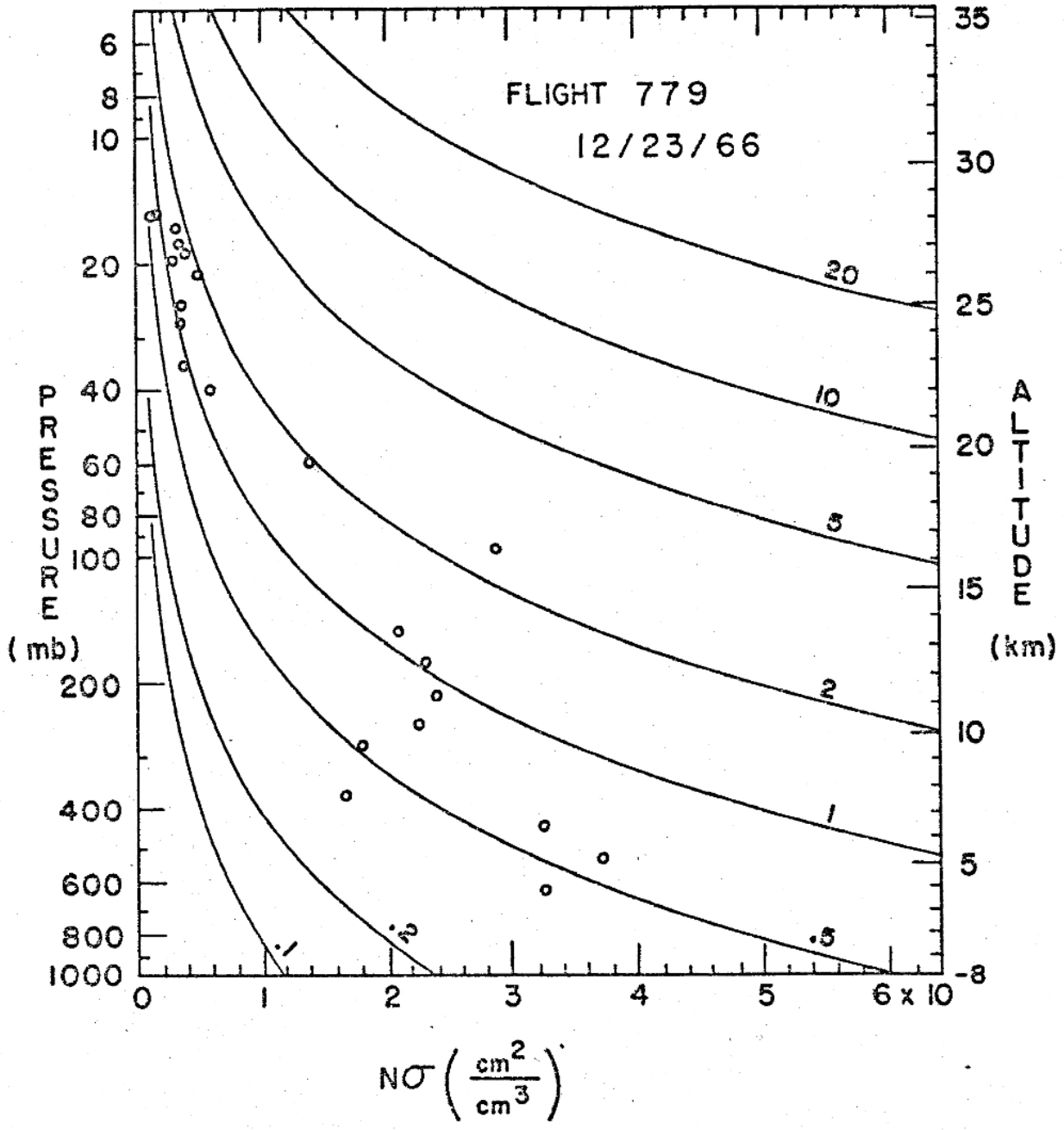
FLIGHT 779
12/23/66
PRESSURE (mb)
ALTITUDE (km)
6
8
10
20
40
60
80
100
200
400
600
800
1000
35
30
25
20
15
10
5
-8
20
10
5
2
1
.5
.2
.1
0
1
2
3
4
5
6 x 10
NσT (cm²/cm³)

Figure 17

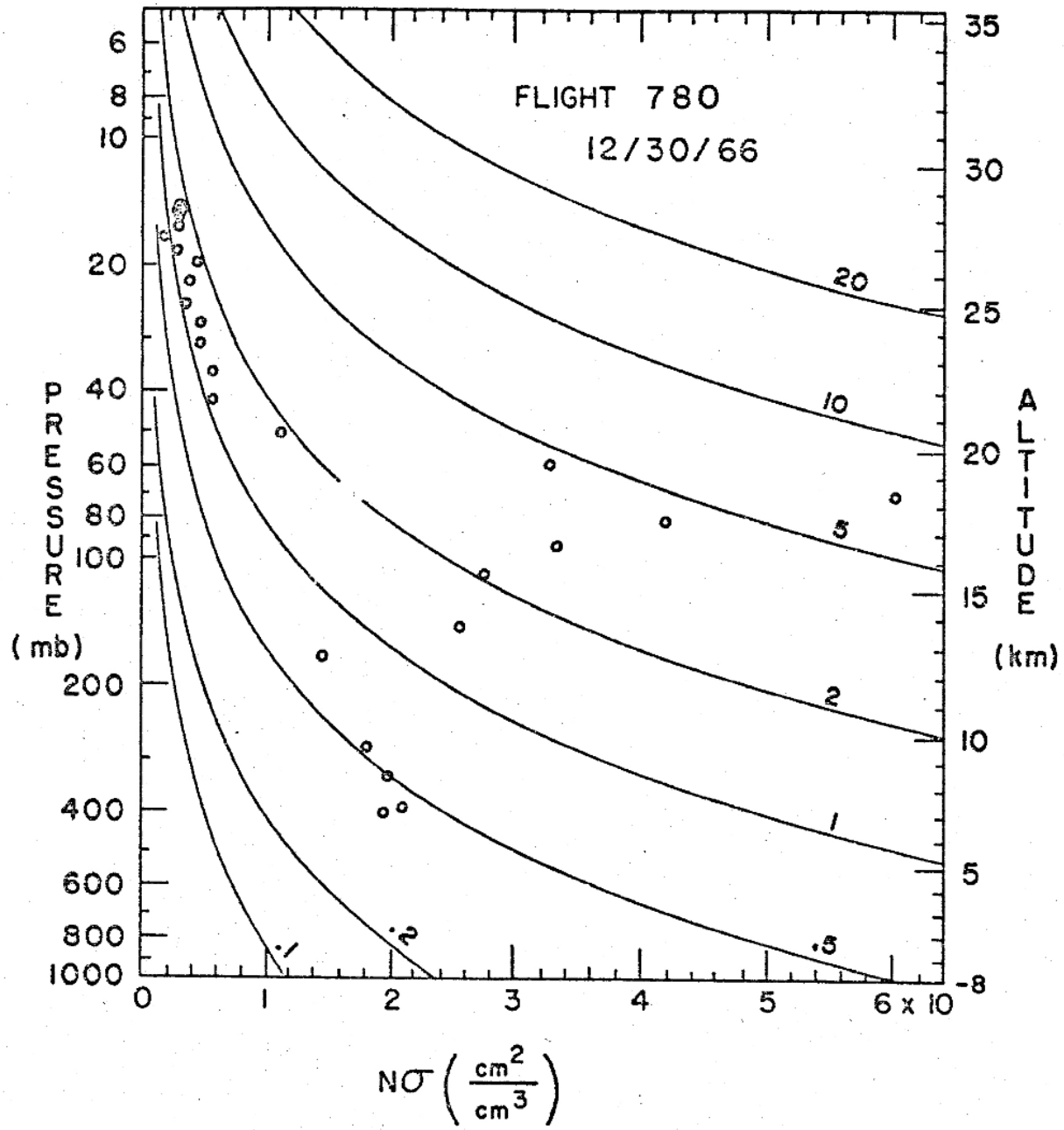
FLIGHT 780
12/30/66
PRESSURE (mb)
ALTITUDE (km)
6
8
10
20
40
60
80
100
200
400
600
800
1000
35
30
25
20
15
10
5
-8
20
10
5
2
1
.5
.2
.1
0
1
2
3
4
5
6 x 10
$N\sigma\left(\frac{cm^2}{cm^3}\right)$

Figure 18

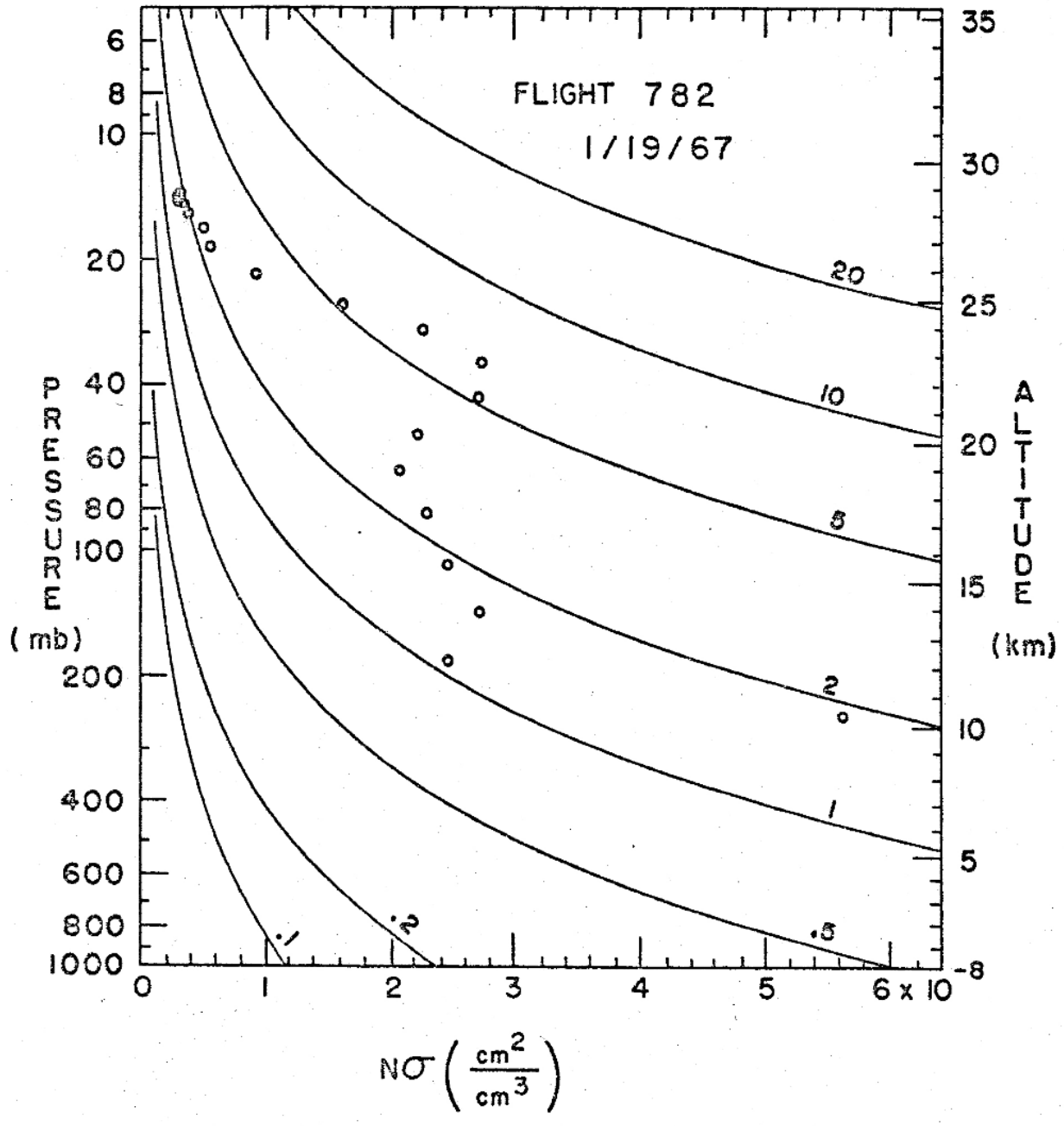
FLIGHT 782
1/19/67
PRESSURE (mb)
ALTITUDE (km)
6
8
10
20
40
60
80
100
200
400
600
800
1000
35
30
25
20
15
10
5
-8
20
10
5
2
1
.5
.2
.1
0
1
2
3
4
5
6 x 10
$N\sigma\left(\frac{cm^2}{cm^3}\right)$

Figure 19

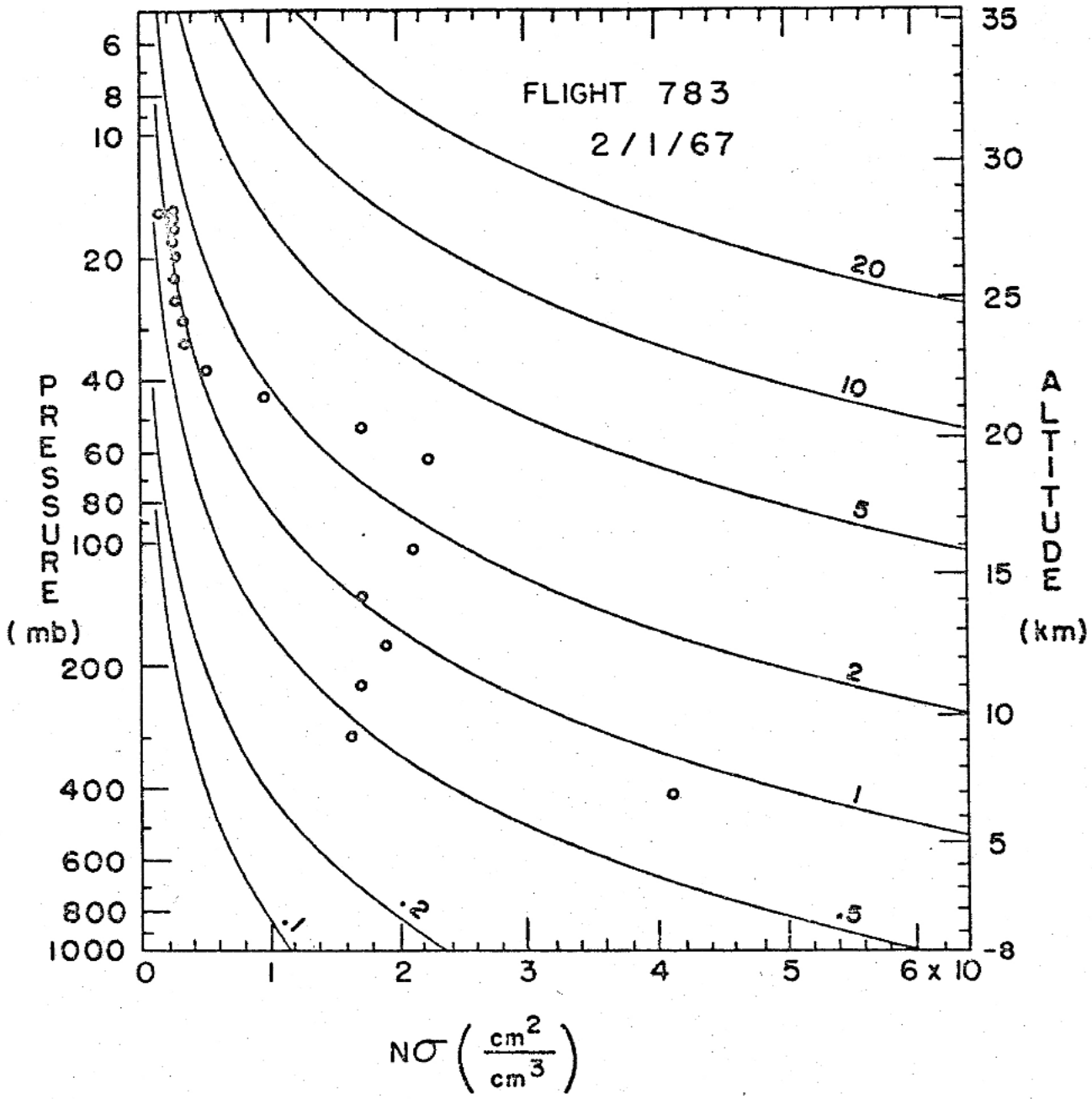
FLIGHT 783
2/1/67
PRESSURE (mb)
ALTITUDE (km)
6
8
10
20
40
60
80
100
200
400
600
800
1000
35
30
25
20
15
10
5
-8
20
10
5
2
1
.5
.2
.1
0
1
2
3
4
5
6 x 10
NO (cm²/cm³)

Figure 20

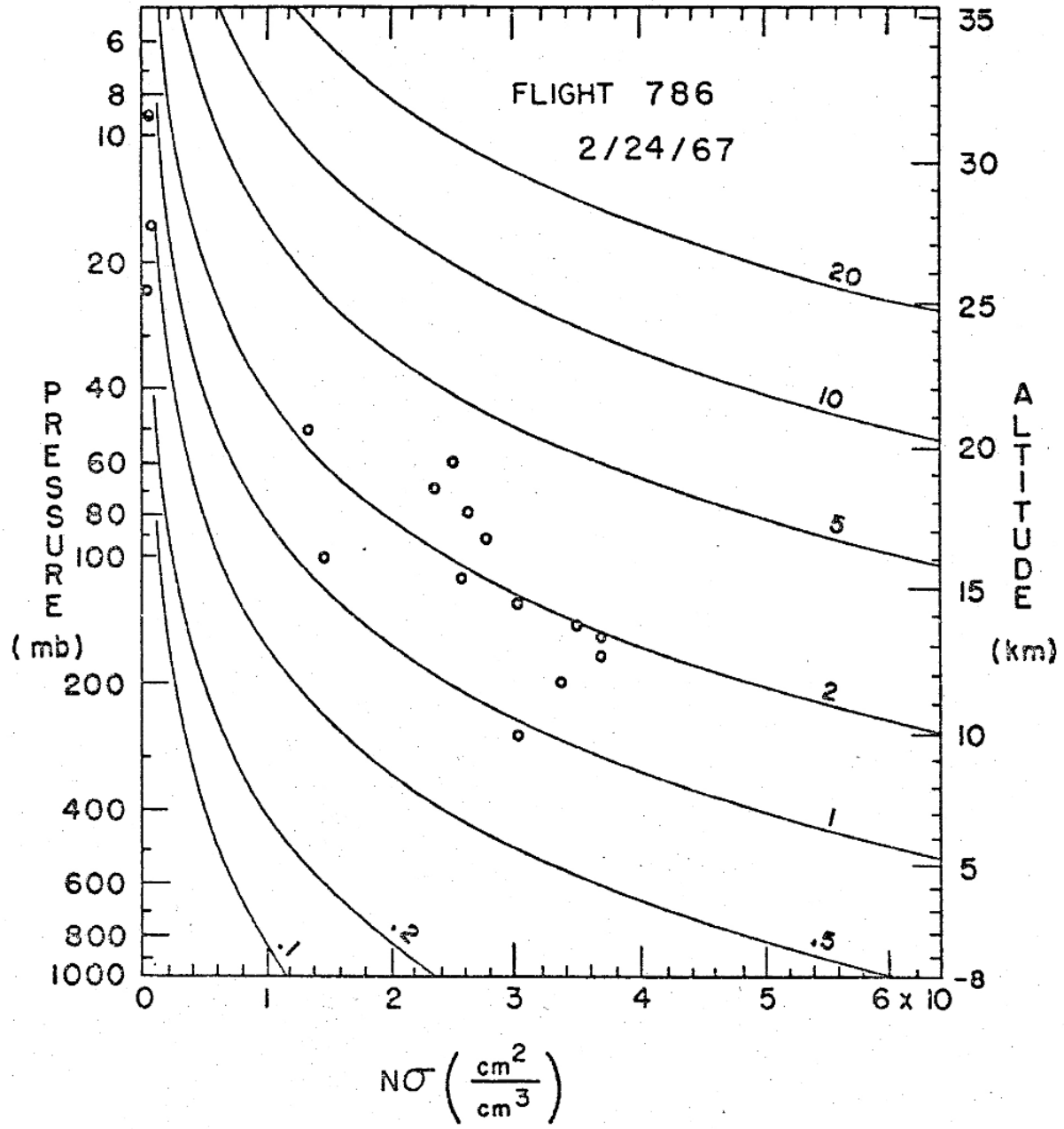
FLIGHT 786
2/24/67
PRESSURE (mb)
ALTITUDE (km)
6
8
10
20
40
60
80
100
200
400
600
800
1000
35
30
25
20
15
10
5
-8
20
10
5
2
1
.5
.2
.1
0
1
2
3
4
5
6 x 10
NO (cm²/cm³)

Figure 21

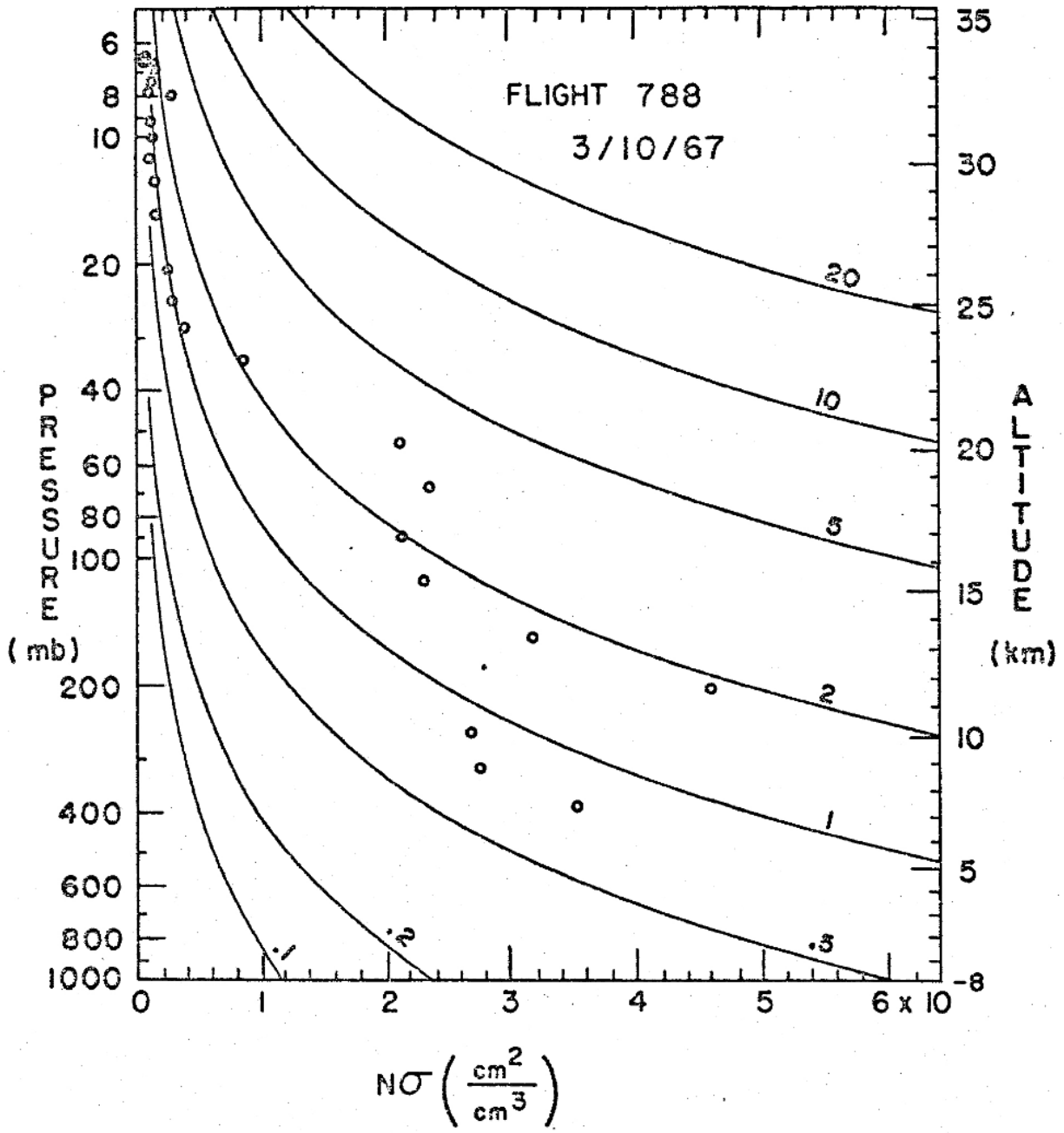
FLIGHT 788
3/10/67
PRESSURE (mb)
ALTITUDE (km)
6
8
10
20
40
60
80
100
200
400
600
800
1000
35
30
25
20
15
10
5
-8
20
10
5
2
1
.5
.2
.1
0
1
2
3
4
5
6 x 10
$N\sigma\left(\frac{cm^2}{cm^3}\right)$

Figure 22

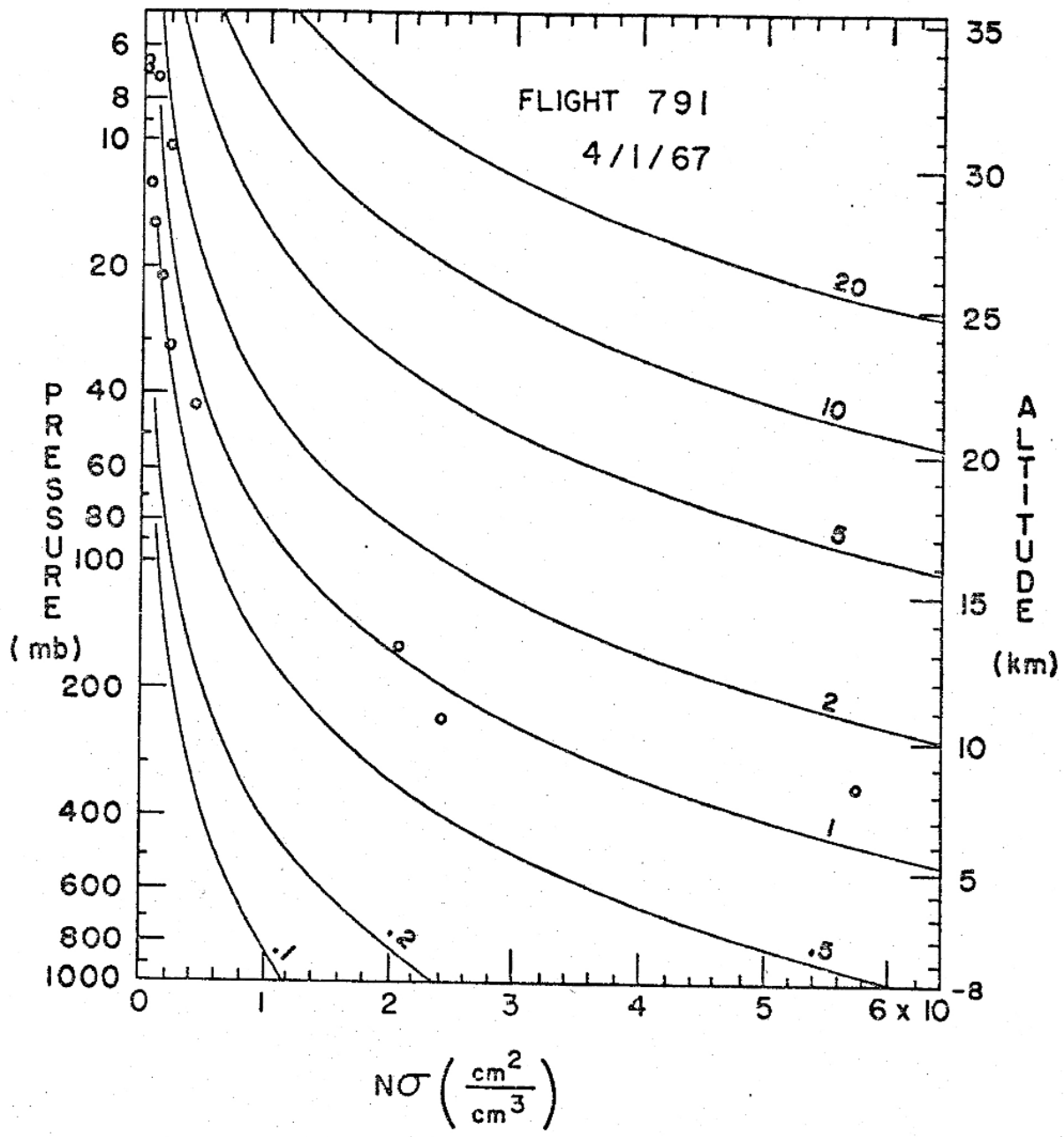
FLIGHT 791
4/1/67
PRESSURE (mb)
ALTITUDE (km)
6
8
10
20
40
60
80
100
200
400
600
800
1000
35
30
25
20
15
10
5
-8
20
10
5
2
1
.5
.2
.1
0
1
2
3
4
5
6 x 10
$N\sigma\left(\frac{cm^2}{cm^3}\right)$

Figure 23

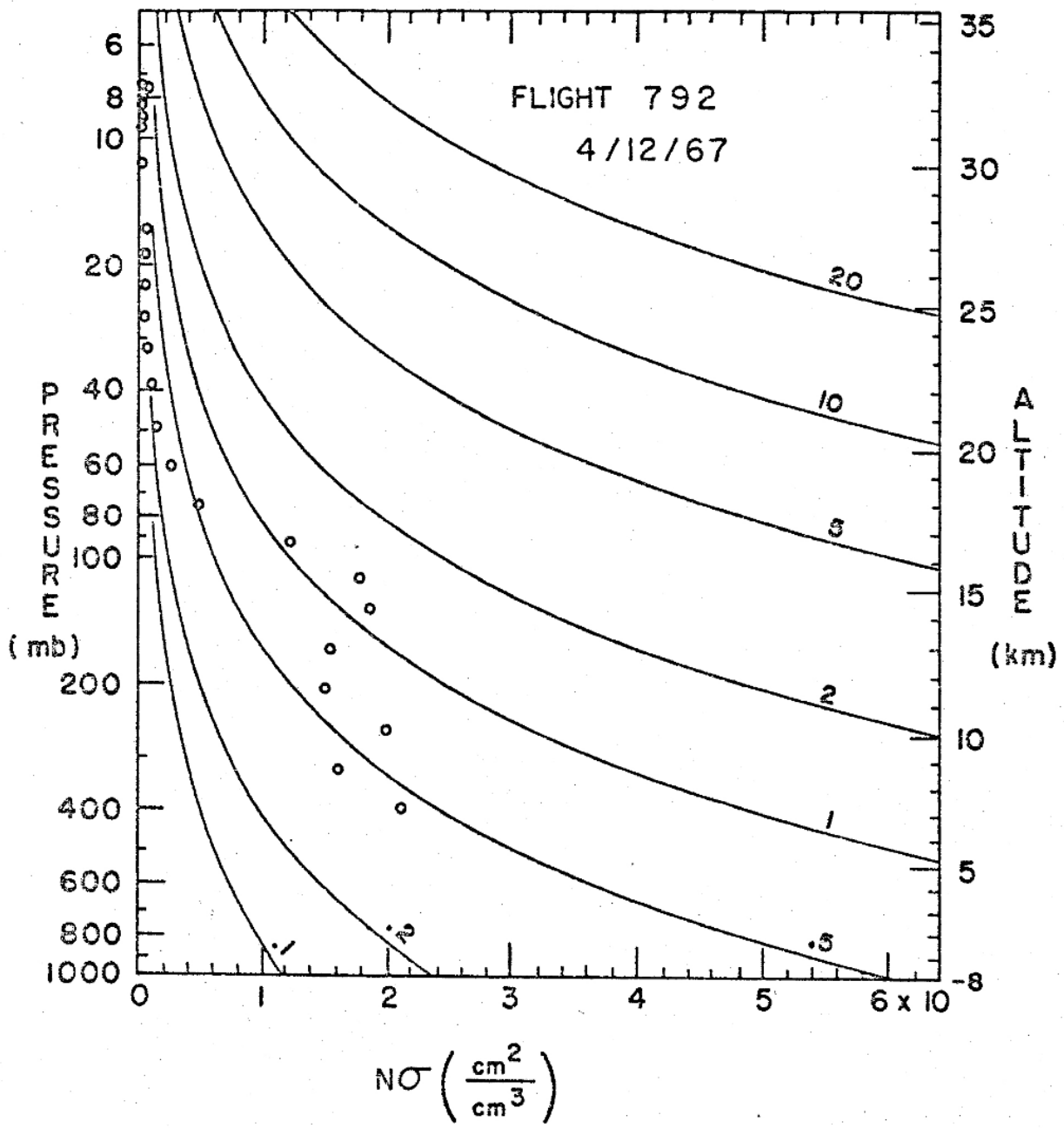
FLIGHT 792
4/12/67
PRESSURE (mb)
ALTITUDE (km)
6
8
10
20
40
60
80
100
200
400
600
800
1000
35
30
25
20
15
10
5
-8
20
10
3
2
1
.5
.2
.1
0
1
2
3
4
5
6 x 10
NO (cm²/cm³)

Figure 24

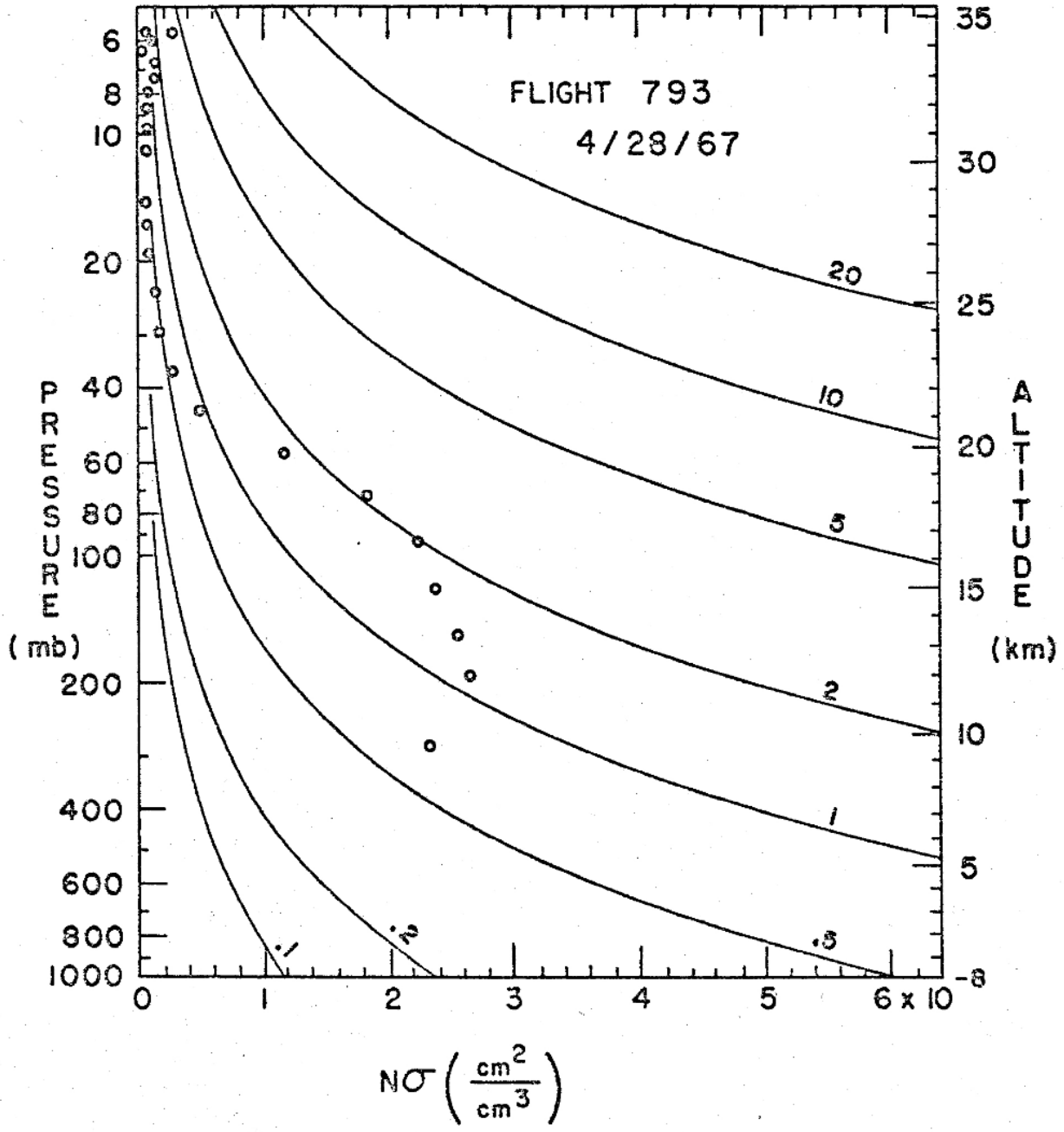
FLIGHT 793
4/28/67
PRESSURE (mb)
ALTITUDE (km)
6
8
10
20
40
60
80
100
200
400
600
800
1000
35
30
25
20
15
10
5
-8
20
10
5
2
1
.5
.2
.1
0
1
2
3
4
5
6 x 10
Nσ (cm²/cm³)

Figure 25

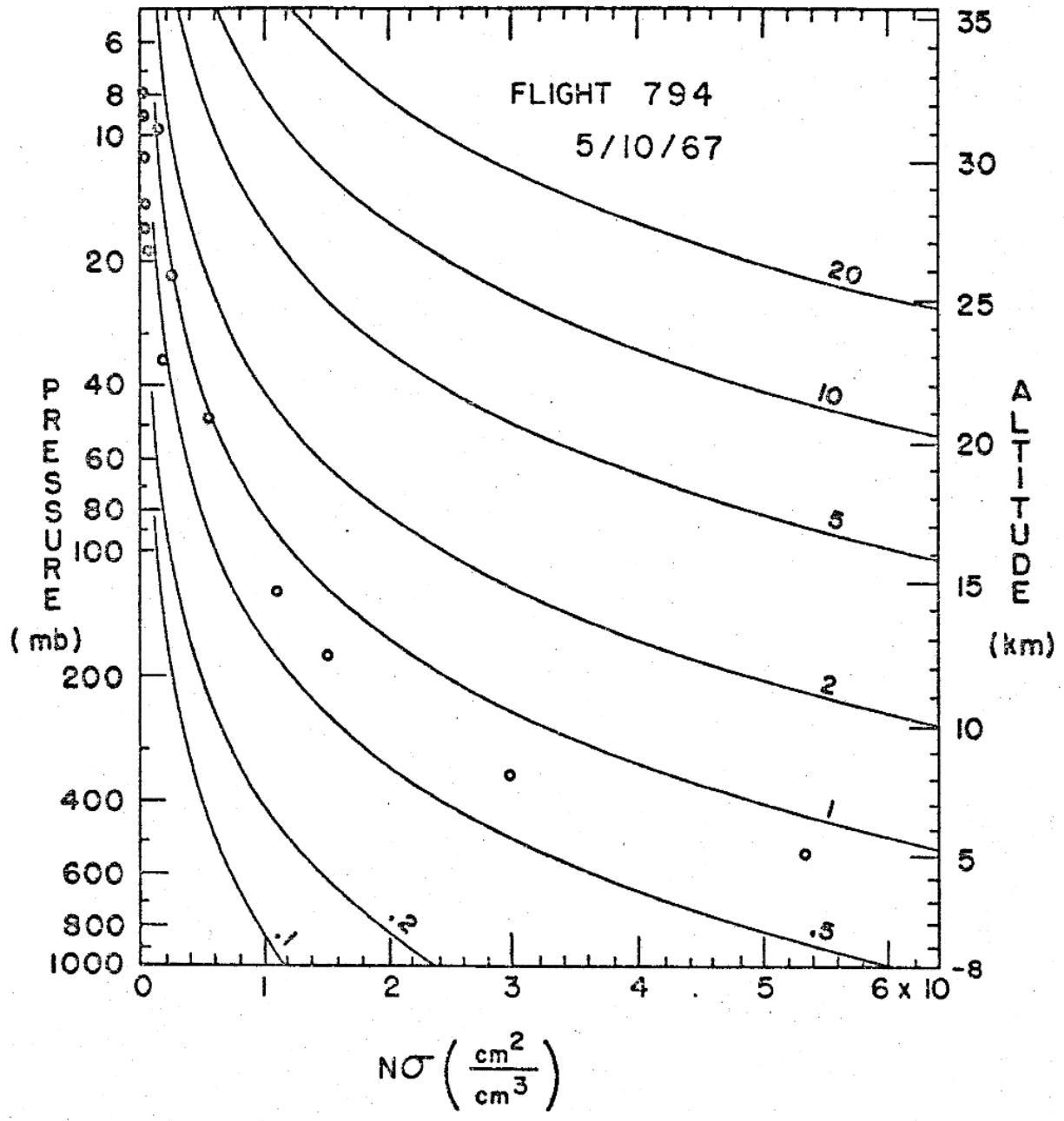
FLIGHT 794
5/10/67
PRESSURE (mb)
ALTITUDE (km)
6
8
10
20
40
60
80
100
200
400
600
800
1000
35
30
25
20
15
10
5
-8
20
10
5
2
1
.5
.2
.1
0
1
2
3
4
5
6 x 10
NO (cm²/cm³)

Figure 26

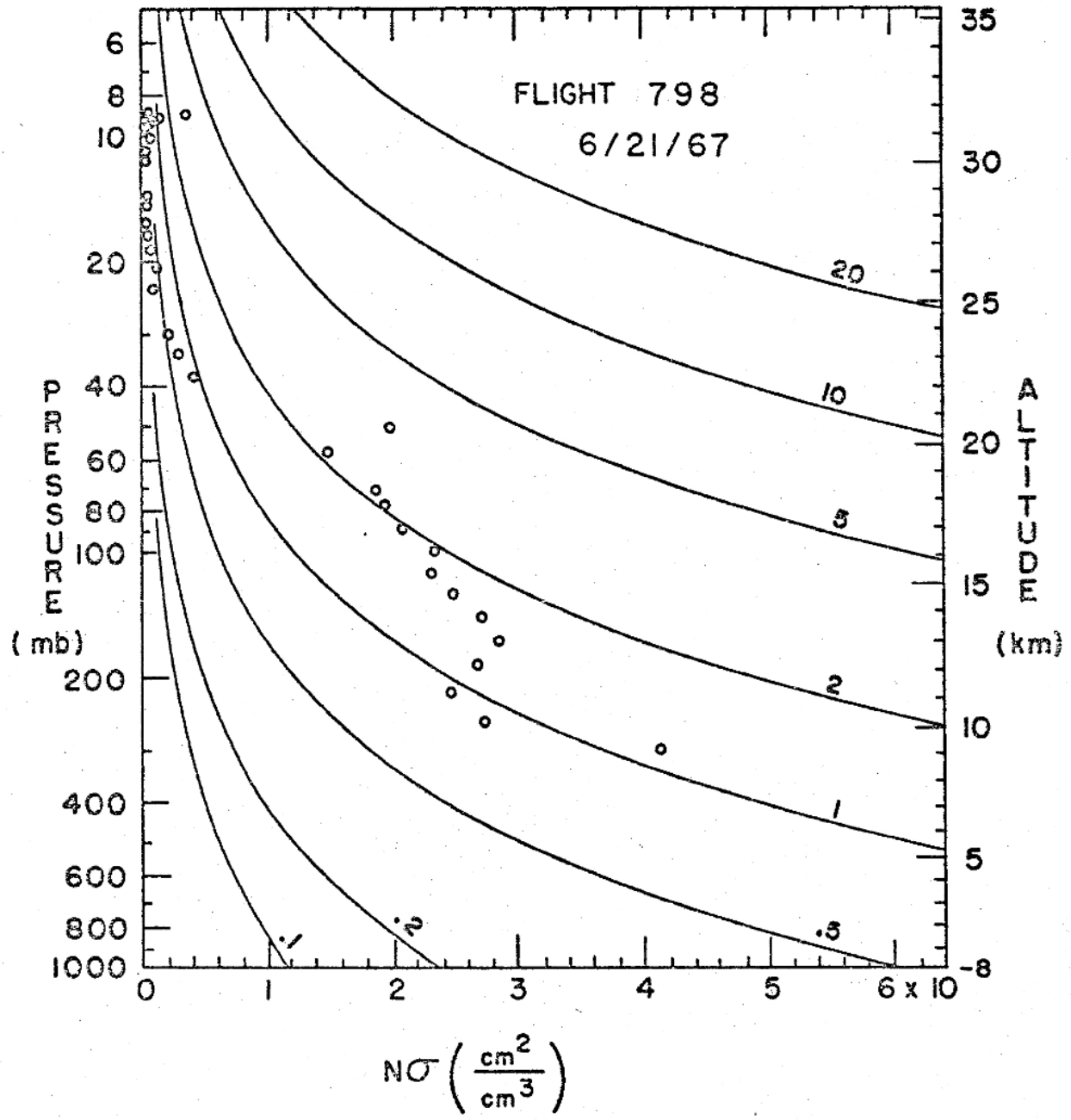
FLIGHT 798
6/21/67
PRESSURE (mb)
ALTITUDE (km)
6
8
10
20
40
60
80
100
200
400
600
800
1000
35
30
25
20
15
10
5
-8
20
10
5
2
1
.5
.2
.1
0
1
2
3
4
5
6 x 10
NσT (cm²/cm³)

Figure 27

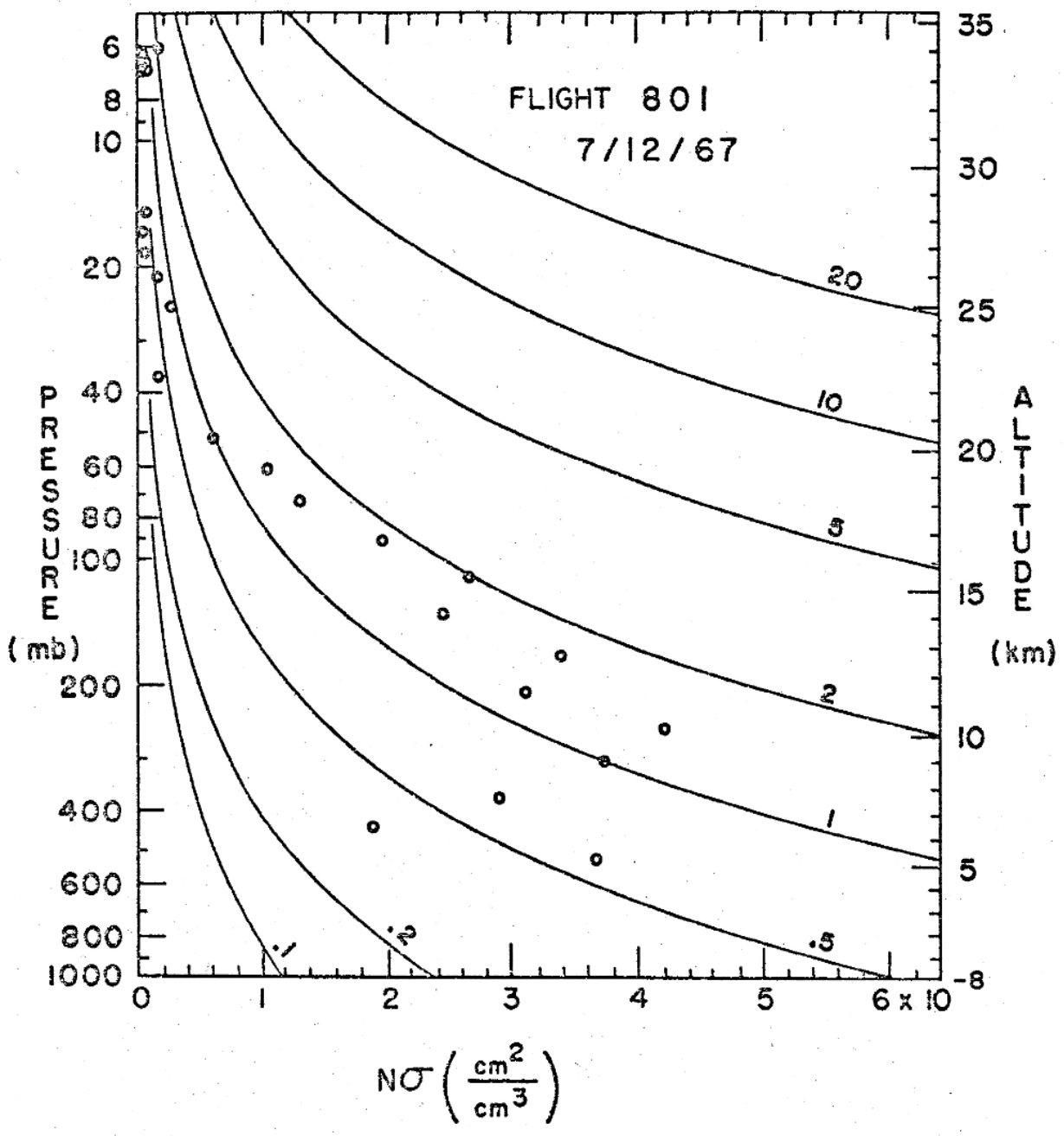
FLIGHT 801
7/12/67
PRESSURE (mb)
ALTITUDE (km)
6
8
10
20
40
60
80
100
200
400
600
800
1000
35
30
25
20
15
10
5
-8
20
10
5
2
1
.5
.2
.1
0
1
2
3
4
5
6 x 10
NσT (cm²/cm³)

Figure 28

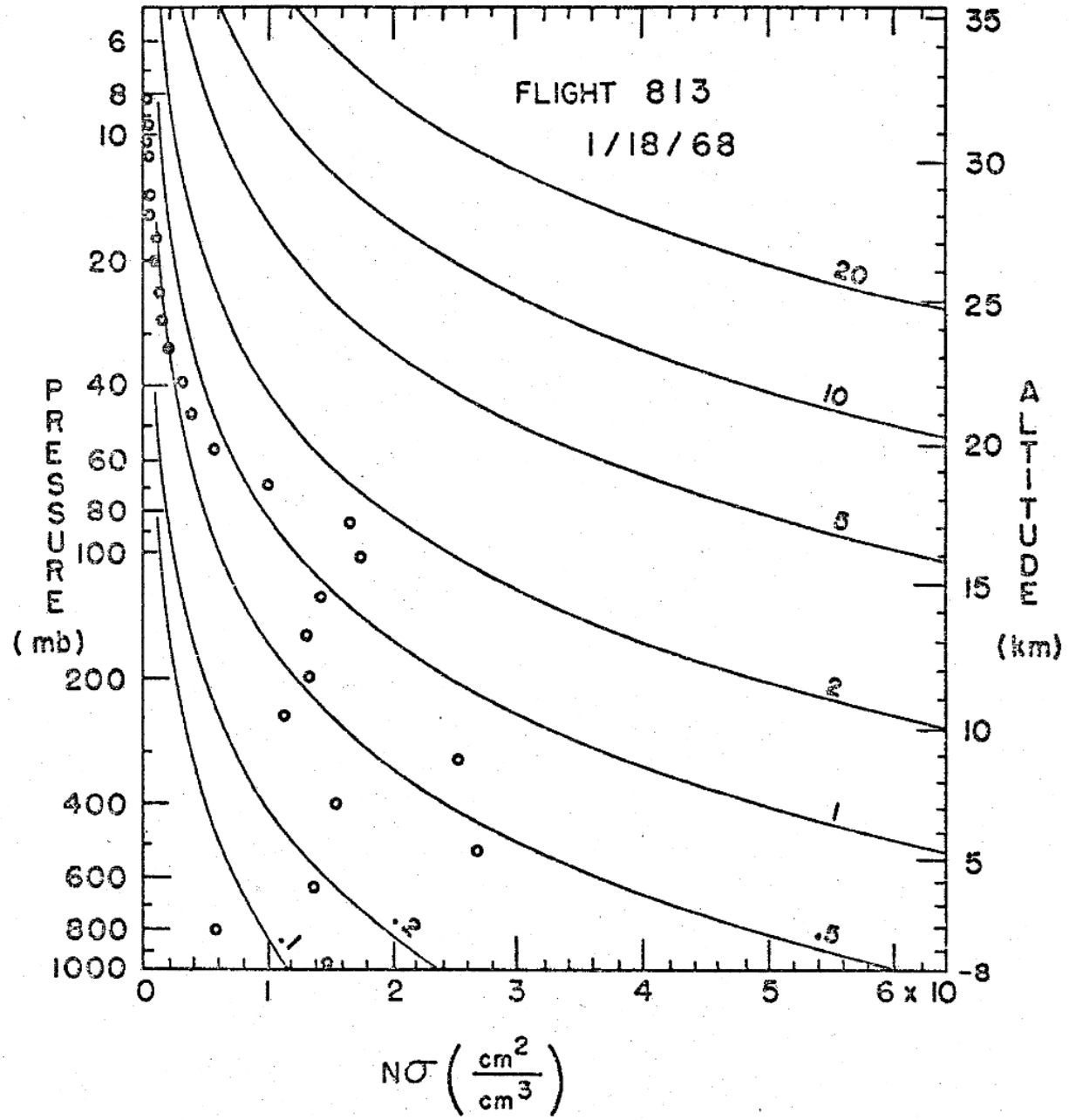
FLIGHT 813
1/18/68
PRESSURE (mb)
ALTITUDE (km)
6
8
10
20
40
60
80
100
200
400
600
800
1000
35
30
25
20
15
10
5
-8
20
10
5
2
1
.5
.2
.1
0
1
2
3
4
5
6 x 10
NσT (cm²/cm³)

Figure 29

average concentration of aerosols along the path. The tangent height of a path through the atmosphere that traverses one air mass is about 26 km and is well above the aerosol maximum.

Figure 30 gives evidence for the apparent systematic change with time of the stratospheric aerosols at mid-latitudes. In 1965 the concentration of aerosols was seen to be decreasing, in the summer of 1966 this trend was seen reversed and in each successive flight until early March 1967 the stratospheric aerosol concentration was found to be increasing. Measurements in the spring and summer of 1967 indicated a continuing decrease of the aerosols during this time and the final flight in this series, Flight 813, made on January 18, 1968, again shows an increase in the aerosols. These variations do not seem to be annual variations.

As has been previously indicated, the maximum concentration observed in this series of flights occurred in February of 1967. The lowest concentration was seen in the late summer of 1967. At an altitude of 26 km this minimum was approximately four times less than the observed maximum.

J. M. Rosen (1969b) has indicated his observation of the decrease in aerosol concentration from 1964 until late 1967. Unfortunately he has no data during the time of the increase in late 1966 and early 1967.

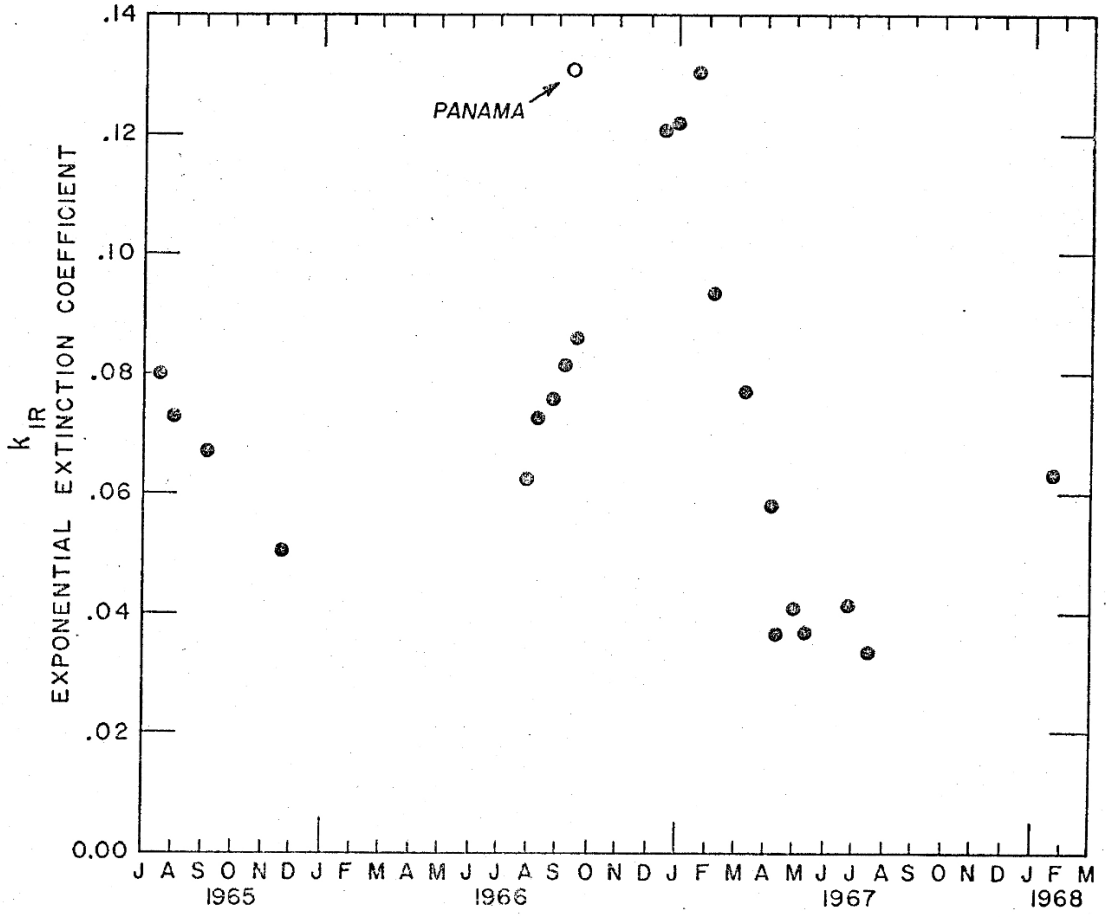

Extinction coef., k_{IR}, determined for the 26 km layer as a function of the time from 1965 to 1968.

Figure 30

J. J. Kosters, T. G. Kyle and D. G. Murcray (1969) have reported from their balloon flights of June 26, 1967 and January 23, 1967 the presence of a much higher concentration of aerosols at the time of the January flight than during the June flight.

The mechanism responsible for the variability of the stratospheric aerosols during this time has previously (Rosen, 1969b) been thought to be due to the decay of the residue volcanic material injected into the stratosphere in the 1963 Bali explosion. The observation of a systematic change in the concentration of stratospheric aerosols by a factor of 4 in a period of only months casts severe doubt on the credibility of this model.

B. Scattering Properties of the Stratospheric Aerosols.

As was discussed in Section II-B, the slope of the curve of intensity as a function of air mass for the infrared sensitive telescope D is related to the aerosol concentration at the tangent height of the ray that traverses the indicated air mass. This slope is called the exponential extinction coefficient, k. The exponential extinction coefficients for the shorter wavelength telescopes B and A similarly reflect the presence of the atmospheric aerosols, but with less sensitivity, since the extinction at shorter wavelengths is primarily due to the molecular component of the atmosphere.

The data from telescopes A, B and D allow the determination of the wavelength dependence of the scattering produced by the stratospheric aerosols.

For example, consider the data from telescopes A, B and D from Flight 813 (January 18, 1968). This flight was made at a time of high aerosol concentration as is indicated by Figure 30. Figure 31 shows a plot of the observed intensities from this flight as a function of the number of atmospheres along the ray traversing the atmosphere at the time the intensity was observed. From this figure at 2 atmospheres of air mass one notes the exponential extinction coefficients as summarized in Table III.

Table III

(Flight 813)

Telescope	λ [μ]	k_{total}	k_R
A	.367	.75	.51
B	.430	.46	.26
D	.910	.09	.012

The top curve of Figure 32 illustrates a plot of these total extinction coefficients k_{total}, as a function of wavelength λ, on a log-log plot. Subtraction of the extinction coefficient for each wavelength due to the

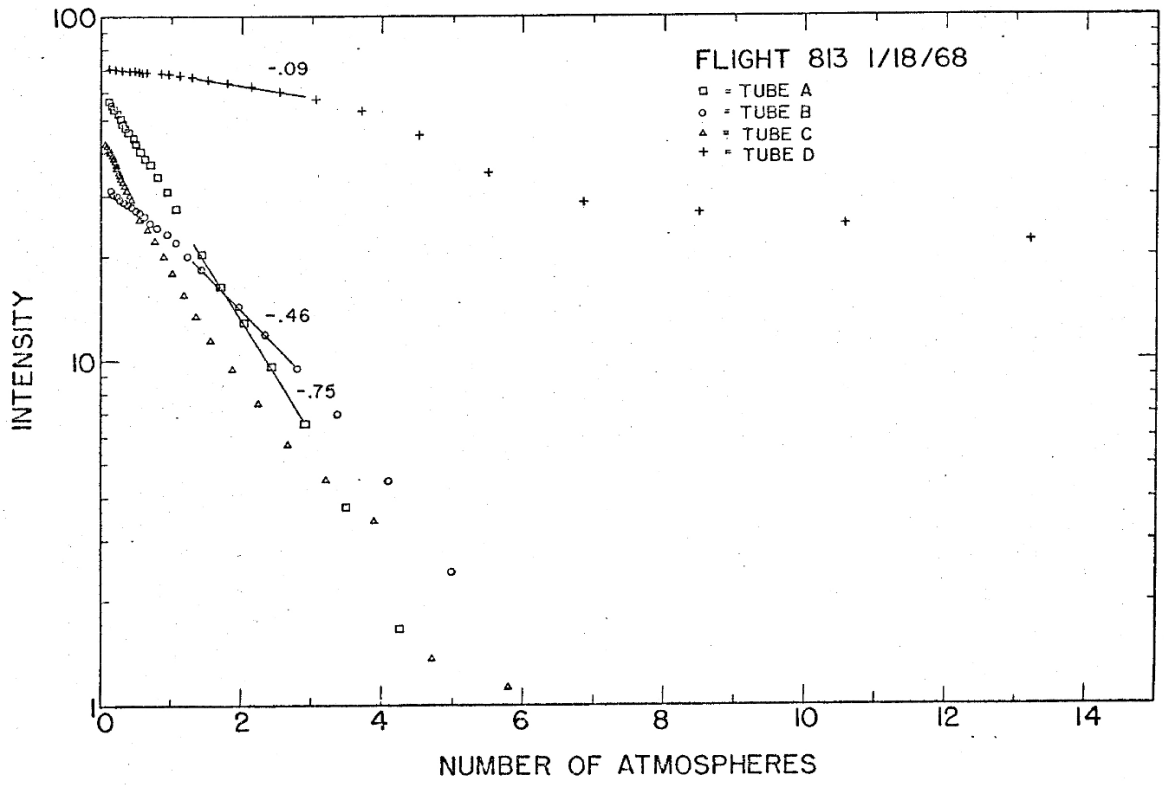

Intensity as a function of atmospheric path for Flight 813.

Figure 31

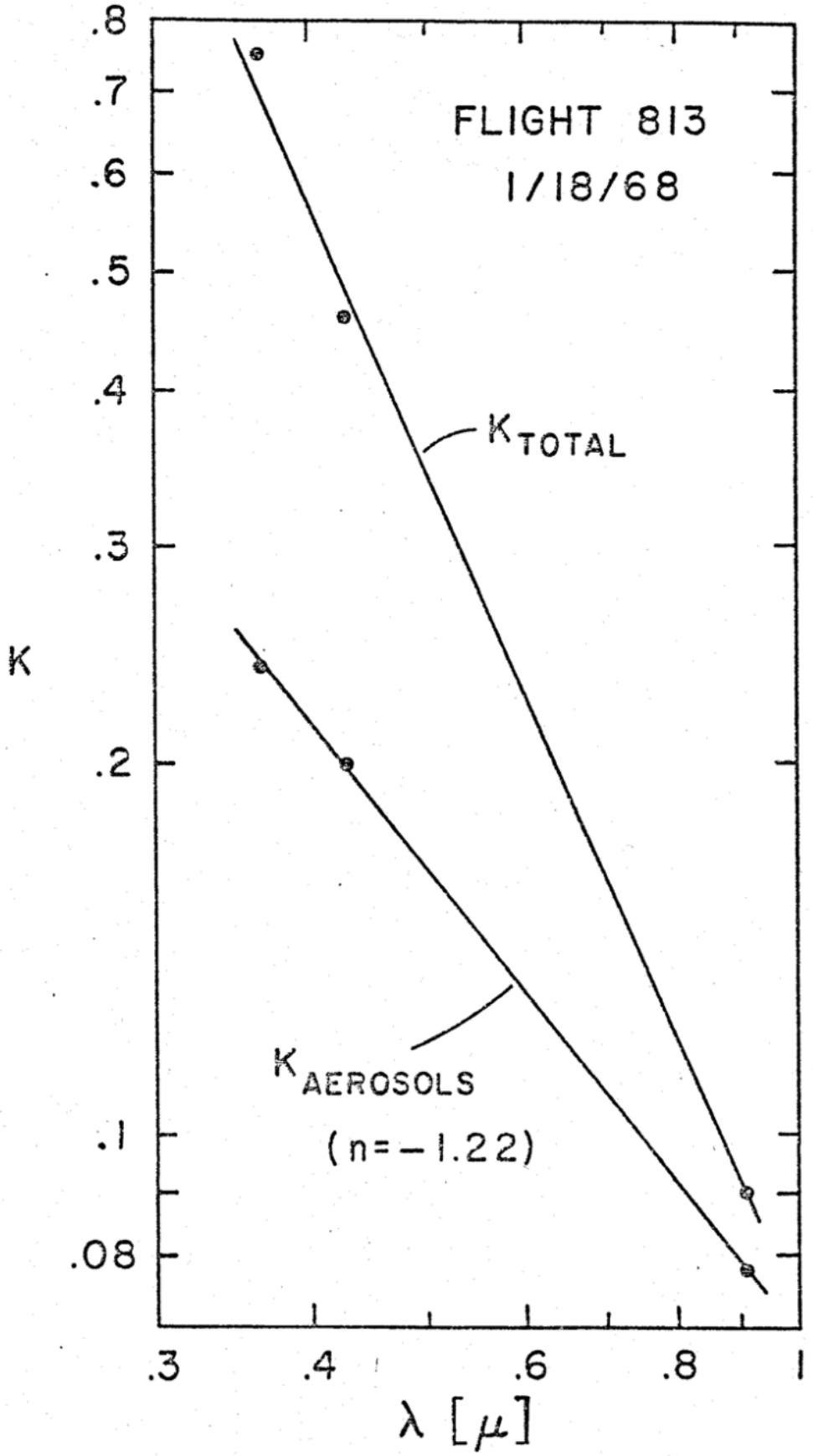

Exponential extinction coefficient at 2 atmospheres of path as a function of wavelength.

Figure 32

molecular component of the atmosphere, k_R, (Allen, 1963) yields the extinction coefficients for each wavelength as indicated on the lower curve of Figure 32. Assuming a power law for the wavelength dependence of the extinction coefficient of the aerosols, $k \propto \lambda^n$, leads to $n = -1.2$ for this flight.

Similar analysis was performed on the data from each of the flights summarized in Table II on page and the resulting n's are plotted on Figure 33 above the date for each flight along with estimates of the errors associated with each point. The larger errors associated with the determined n's for the flights in the spring and summer of 1967 reflect the small concentration of aerosols found to be present in the stratosphere at that time.

Insight into the significance of these results is obtained by considering the expected extinction as a function of wavelength from a distribution of aerosols that has a number density as a function of particle size, N(r), such that

$$N(r) \propto r^{\alpha}$$

where r is the radius of the aerosols. For such a distribution one finds

$$dN = C\, r^{\alpha-1}\, dr$$

particles present per cm^3 in the size range dr where C is a constant.

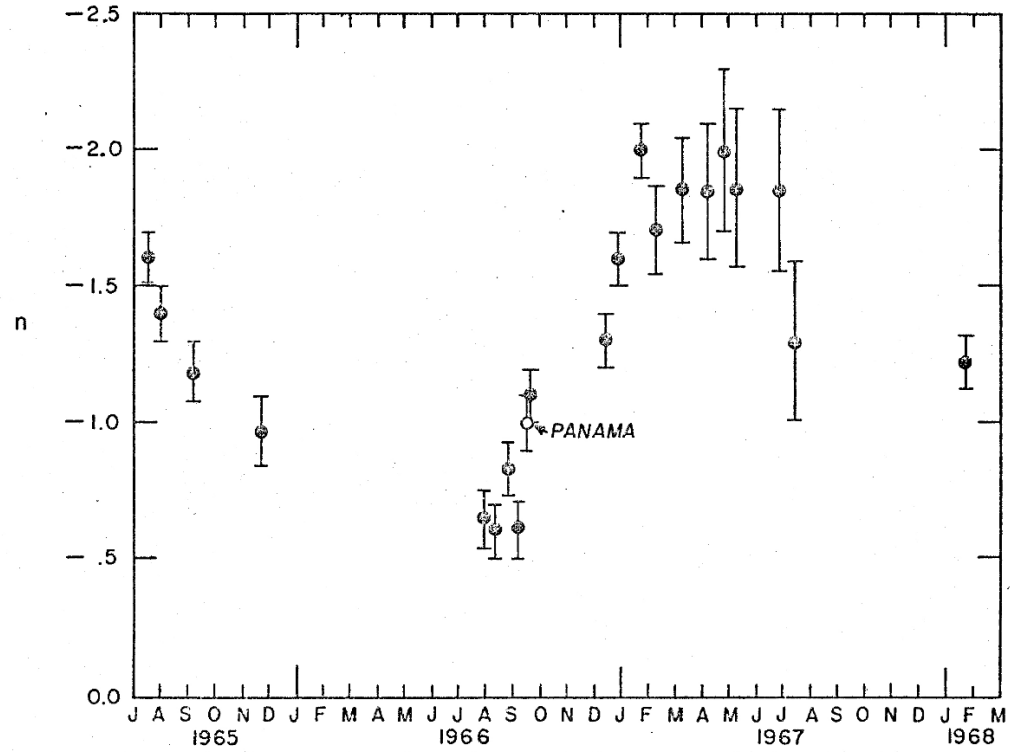

Exponent of the determined power law dependence of the exponential extinction coefficient of the stratospheric aerosols on wavelength vs. the date of the measurement.

Figure 33

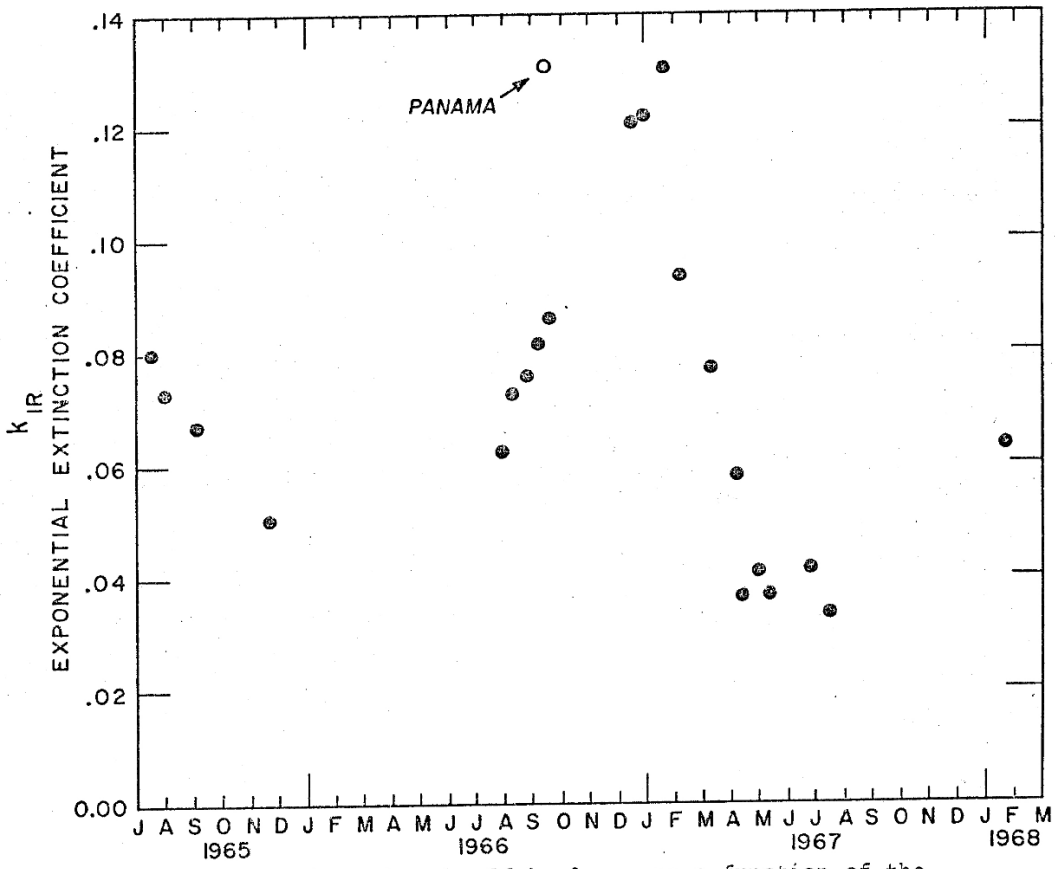

Extinction coef., k_{IR}, determined for the 26 km layer as a function of the time from 1965 to 1968.

Figure 30

For a power law distribution in particle size one can show that the total extinction coefficient, k', (the total cross-section per cm^3) has the same wavelength dependence no matter what the form of extinction curve, Q(r), for the particles. This can be seen since

$$k'(\lambda) = \int \pi r^2 \, Q(r) \, dN.$$

Thus, by substitution

$$k'(\lambda) = \pi \, C \int_0^{\infty} r^{\alpha+1} \, Q \left(\frac{2\pi r}{\lambda} \right) dr$$

or changing variables

$$k'(\lambda) = \pi \, C \left(\frac{\lambda}{2\pi}\right)^{\alpha+2} \int_0^{\infty} x^{\alpha+1} \, Q(x) \, dx.$$

If this integral converges*, one then has that the wavelength dependence of the total extinction

$$k' \propto \lambda^h$$

is such that

$$n = \alpha + 2.^{\dagger}$$

*For the case of small dielectric spheres, H. C. Van De Hulst (1962) has demonstrated the convergence of the integral when $-6 < \alpha < -2$.

†Volz (1954) has given the empirical finding that n=-1 to -2 gives $\alpha = -3$ to -4. He has also made numerical integrations with limits other than 0 and ∞.

Referring to the data presented on Figure 33, the exponent of the power law size distribution varies between -2.6 and -4 and is in the range reported by Junge (1963). During the decrease in the concentration in the last half of 1965 the size distribution of the aerosols was observed to be flattening. This may be indicative of a coagulation of the resident stratospheric aerosols. In the later summer and fall of 1966 when the concentration of the aerosols was seen to be increasing the size distribution remained flat for almost two months and then became steeper. In the spring of 1967 as the concentration decreased the size distribution remained steep and gradually flattened again perhaps giving some evidence for coagulation taking place.

The open point on Figure 33 is from the data of Flight 774 over Panama. The size distribution for the aerosols above Panama was seen to be similar to those at the latitude at Minneapolis even though the concentration was several times higher.

VII. The Ozone Problem.

Using the data from telescope C, which is centered at 5950°A in the middle of the Chappuis absorption band of ozone, one should be able to determine the ozone concentration as a function of altitude by using analysis similar to that which has been described to determine the aerosol concentration.

The extinction observed with telescope C is principally due to the absorption of ozone, but in part it is also due to molecular scattering and scattering from the atmospheric aerosols. The amount of extinction from these components can be subtracted from the total observed extinction using the data from the other telescopes to determine the extinction as a function of wavelength for the aerosols since the molecular extinction or Rayleigh scattering is known.

A. The Sunrise Effect. A significant extinction is produced by the ozone which is above the altitude of the balloon. The data from all of the sunrise extinction flights indicate that the extinction produced by the ozone near the balloon's altitude and above the balloon does not follow Beer's law. Examples of this can be seen in the data of telescope C of Flight 792 presented in Figure 4, and that from Flight 813 seen in Figure 31.

The observation of non-exponential extinction could indicate that the ozone above the balloon is diminishing with time or that the absorption cross-section of this atmospheric component is either pressure or temperature dependent.

The apparent non-exponential extinction seems not to be an instrumental effect since telescope C employs construction identical to the other telescopes using the same type vacuum phototube as the A and B telescopes.

Only its filter, which determines its wavelength, is different. In the early sunrise flights wratten filters were used. Later instruments employed glass filters with the same transmission spectral characteristics. The data from the A and B telescopes for all of the flights demonstrate the exponential extinction behavior for the molecular component of the atmosphere.

Experimental evidence by Vigroux (1953) and Humphrey and Badget (1947) indicate the absence of pressure and temperature effects on the cross-section for the Chappuis band. No lines are resolved in the Chappuis band and therefore it seems unlikely that it has a non Beer's law type of band transmission.

Calculations have been made for layers of ozone just above the balloon to see if the presence of a thin concentrated layer of ozone could produce the observed extinction. The absorption in a 2 km thick layer just above the balloon would not account for the observed extinction by almost a factor of two. The effect of a thicker layer or a layer at higher altitude is to reduce the difference of extinction between different elevation angles.

To check to see if the sun reduces the ozone above the balloon after or during sunrise two balloon flights, Flight 823 and Flight 824, were made using standard extinction instruments. The first of these flights was

a sunset experiment on November 17, 1969 followed on November 18 by a sunrise flight. If the effect described above is indeed produced by sunlight on the ozone above the balloon, one should not expect to see it in the sunset experiment. The data from the ozone sensitive tubes for the two flights as a function of the airmass is shown in Figure 34. In the sunset experiment the high altitude ozone above the ozone maximum is observed to produce an exponential extinction. This indicates a constant mixing ratio of the ozone above the ozone maximum which is seen to be at an altitude of about 25 km., the altitude of the tangent ray traversing 1.4 atmospheres of airmass.

The data from the sunrise flight 824 when fit with the exponential extinction coefficient observed in the sunset flight 823, indicates a 27% change in the ozone above the balloon due to the sunrise effect. Since at balloon altitude of 33 km the balloon is above all but about 15% of the ozone in the atmosphere, the sunrise effect should only be expected to produce about a 4% change in the total ozone. Mantis (1970) has looked for the change in the total atmospheric ozone at sunrise by observing the absorption in the 9.6μ ozone band of the ther radiation from the moon during sunrise. At the time of his observation the moon was near the meridian. He reports that no more than a 2% change in the total ozone could be made compatible with his measurement.

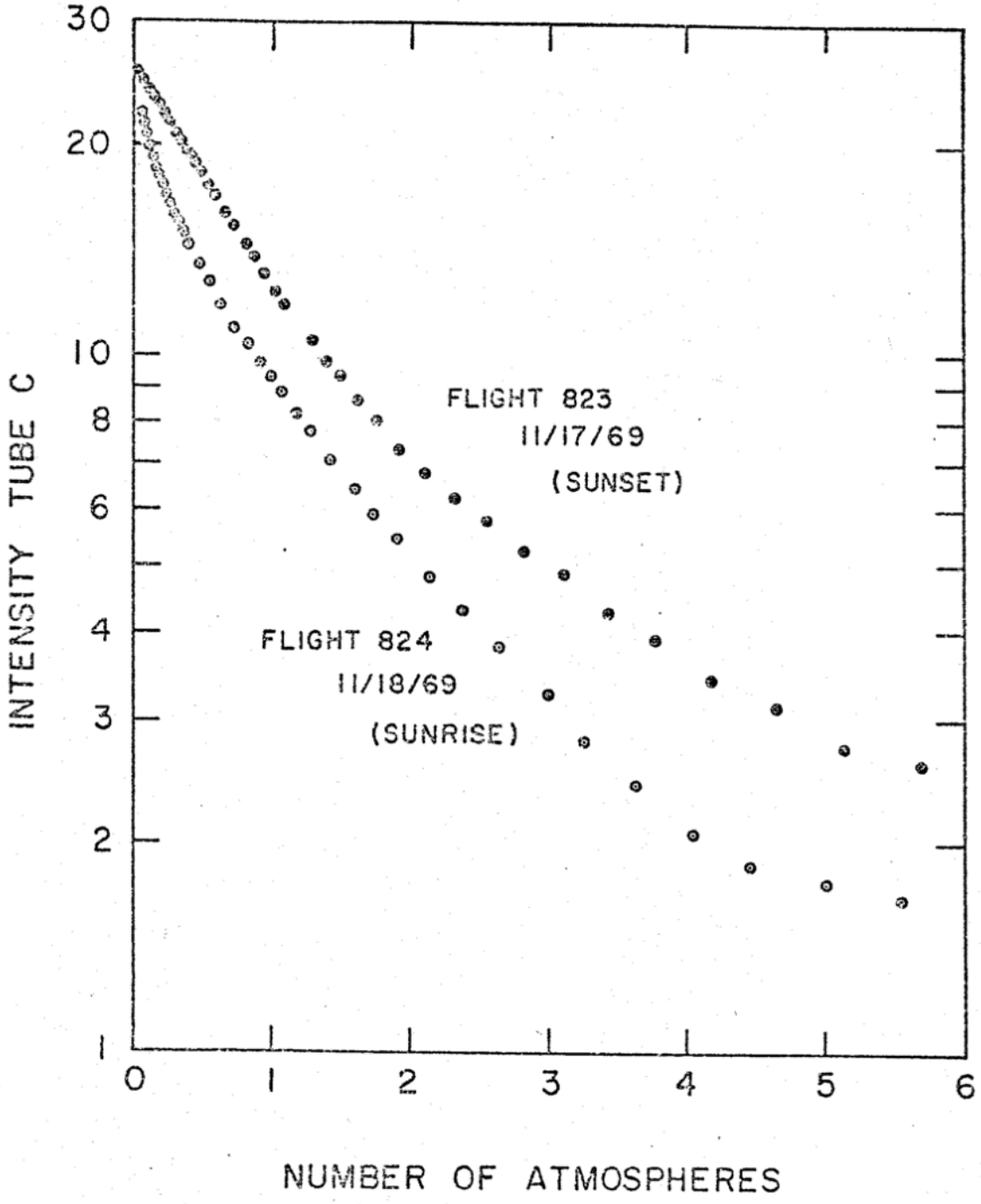
30
20
10
8
6
4
3
2
1
INTENSITY TUBE C
FLIGHT 823
11/17/69
(SUNSET)
FLIGHT 824
11/18/69
(SUNRISE)
0
1
2
3
4
5
6
NUMBER OF ATMOSPHERES

Figure 34

This apparent inconsistency in the two observations perhaps can be explained if some of the ozone from just below the balloon were redistributed in the atmosphere to just above the balloon during the night. It is hoped that future experiments that measure the ozone concentration at balloon altitude during sunrise and future extinction measurements to higher elevation angles will shed light on this problem.

B. The Cross-section Problem. Analysis of the data from the sunrise extinction flight, making allowance for the sunrise effect, produces vertical distribution curves for ozone similar to those that have been reported by Kroening and Ney (1962); however, an absorption cross-section approximately two times smaller than Vigroux's (1953) value of 4.7×10^{-21} cm^2 per atom must be used to find the same order of concentrations as these investigators.

In order to determine the value of the Chappuis cross-section two simultaneous balloon flights (Flight 825 and Flight 826) were made on December 20, 1969. Flight 825 carried an extinction instrument of the type described in this thesis and Flight 826, which was flown by J. Kroening, measured the ozone concentration during ascent before sunset and during descent after sunset. Both of these flights indicate the falloff of the ozone with constant mixing ratio above the ozone maximum.

Unfortunately, the Olland cycle on Flight 825 stopped and the altitude of this flight can only be determined from the extinction data observed with the ultraviolet telescope. Taking into account the possible calibration errors in Kroening's results and the possible errors in determining the altitude of Flight 825 the data indicates that the Chappuis cross-sections should be reduced at least by 2 and perhaps by as much as 6 from Vigroux's value. It is hoped that future experiments will determine the value of the cross-section with considerable more precision.